Inaugural Dissertation

Integration of Olfactory Bulb Output in the Zebrafish Telencephalon analyzed by Electrophysiology and 2-Photon Ca^{2+} - Imaging

submitted to the
Combined Faculties for the Natural Sciences and for Mathematics
at the University of Heidelberg, Germany

for the degree of Doctor of Natural Sciences

presented by

FRANCISCA V. SAINT PAUL, MSc

born in

DUBLIN, IRELAND

2009

The work presented in this thesis was carried out at the Max-Planck-Institute for Medical Research, Department of Biomedical Optics; Heidelberg, Germany and the Friedrich Miescher Institute for Biomedical Research, Novartis Research Foundation; Basel, Switzerland under the supervision of PD Dr. Rainer W. Friedrich.

About half of the results presented here have been published recently in
Yaksi E*, von Saint Paul F*, Niessing J, Bundschuh ST, Friedrich RW (2009) Transformation of odor representations in target areas of the olfactory bulb. *Nature Neuroscience* **12**: 474 – 482 (* Equal contribution)

First Referee: PD Dr. Rainer W. Friedrich
Friedrich Miescher Institute for Biomedical Research
Basel, Switzerland

Second Referee: Prof. Dr. Peter H. Seeburg
Max-Planck-Institute for Medical Research
Heidelberg, Germany

Herewith I declare that I prepared the present work on my own and with no other sources and aids than quoted.

Basel, April 2009

SUMMARY

To understand how the brain generates representations of the external world it is crucial to analyze the processing of sensory information between early processing centers and higher brain regions. In the first olfactory relay, the olfactory bulb (OB), odors are represented by dynamic patterns of activity across the population of principal neurons, the mitral cells. During an odor response, subsets of mitral cells synchronize their action potentials and convey information that is different from the information contained in non-synchronized firing patterns. It is, however, poorly understood how these combinatorial representations are further processed in higher brain areas. I used a small vertebrate model system, the zebrafish, to examine how neurons in the dorsal posterior telencephalon (Dp), a direct target of OB output that is homologous to olfactory cortex, extract information from OB output activity patterns. Using 2-photon Ca^{2+} - imaging and whole-cell patch-clamp recordings, I found that individual Dp neurons receive input from diverse sets of mitral cells. Unlike in mitral cells, responses of Dp neurons to binary mixtures of odors could not be predicted from their responses to the components. Electrophysiological and pharmacological results demonstrated that suprathreshold responses are controlled by the convergence of excitatory and inhibitory pathways in single Dp neurons. I next analyzed the temporal integration properties of neurons and neuronal circuits to examine whether neurons in Dp may selectively extract the information contained in synchronized mitral cells spikes. No evidence for coincidence detection mechanisms was found; rather, action potential firing is controlled primarily by a slow membrane depolarization. In conclusion, the readout of information in Dp is determined by a balance of slow excitatory and inhibitory inputs that allows Dp neurons to detect defined patterns of excitation and inhibition across the population of mitral cells in the olfactory bulb. This mechanism does not depend on the synchronization of inputs and mediates the association of information about multiple molecular features of an odor stimulus. Together, these data suggest that neurons in Dp form synthetic representations of olfactory objects.

ZUSAMMENFASSUNG

Um zu verstehen, wie das Gehirn eine interne Repräsentation der externen Welt generiert, ist es notwendig, die Verarbeitung sensorischer Information zwischen peripheren Zentren und höheren Hirnarealen zu untersuchen. Im ersten olfaktorischen Verarbeitungszentrum, dem Bulbus olfactorius (OB), werden Gerüche durch dynamische Aktivitätsmuster von Mitralzellen repräsentiert. Während einer Geruchsantwort synchronisieren Gruppen von Mitralzellen ihre Aktionspotenziale und transportieren Stimulusinformation, die sich von der Information in nicht synchronisierten Feuermustern unterscheidet. Die weitere Verarbeitung dieser kombinatorischen Repräsentationen in höheren Hirnarealen ist jedoch noch kaum verstanden. Ich habe ein kleines Wirbeltiermodell, den Zebrafisch, verwendet, um zu untersuchen, wie Neurone im posterioren dorsalen Telencephalon (Dp), einem dem olfaktorischen Cortex homologen Projektionsgebiet des OB, Information aus Aktivitätsmustern im OB extrahieren. Mithilfe von 2-Photonen Ca^{2+} - Imaging und intrazellulären Ableitungen einzelner Zellen habe ich herausgefunden, dass einzelne Dp Neurone Inputs von mehreren Mitralzellen erhalten. Im Gegensatz zu Mitralzellen konnten die Antworten der Dp Neurone auf binäre Geruchsmixturen nicht anhand der Antworten auf die Komponenten vorhergesagt werden. Elektrophysiologische und pharmakologische Experimente zeigten, dass überschwellige Antworten durch die Konvergenz erregender und inhibitorischer Synapsen kontrolliert werden. Untersuchungen der zeitlichen Integrationseigenschaften von Neuronen und Schaltkreisen lieferten keinerlei Hinweise dafür, dass Dp selektiv Information ausliest, die durch synchronisierte Aktionspotentiale transportiert wird. Vielmehr scheint das Feuern von Aktionspotenzialen in Dp primär durch eine langsame Membrandepolarisation bestimmt zu sein. Das Auslesen von Information in Dp ist daher durch ein Gleichgewicht langsamer erregender und hemmender Inputs bestimmt, das es Dp Neuronen ermöglicht, definierte Mitralzell-Aktivitätsmuster zu detektieren. Dieser Mechanismus hängt kaum von der Synchronisation der Eingänge ab und vermittelt die Assoziation zwischen verschiedenen molekularen Determinanten eines Geruchsstimulus. Diese Daten weisen darauf hin, dass Neurone in Dp synthetische Repräsentationen olfaktorischer Objekte erzeugen.

TABLE OF CONTENTS

ACKNOWLEDGEMENTS

I thank PD Dr. Rainer Friedrich for the opportunity to pursue this interesting investigation in his laboratory and under his supervision, for lots of suggestions for the data analysis and for his support and motivating discussions particularly in the final stage of my PhD. Thank you to all the Friedrich lab members for the nice working atmosphere and particularly to Eddie, Martin, and Sebastian who always were supportive from my first day in the lab until the end.

I thank Prof. Seeburg for taking the time to review and evaluate my thesis and Prof. Frings and Prof. Schuster for their agreements to be members of my examination committee. Furthermore I thank the physicists in the BMO Department for helping me understand some of the theoretical backgrounds from a different angle.

This project was supported by the German Research Foundation (GK 791), the Novartis Research Foundation and the Max-Planck-Society.

INTRODUCTION

A challenging question in neuroscience is to understand how information about the outside world is represented and processed by the activity of large populations of neurons. Vision, hearing, touch, taste and olfaction are the five modalities via which we perceive our external environment. All of these – except for olfaction – relay primary sensory input to the thalamus from where it is subsequently mapped onto the cerebral cortex. Olfactory input, in contrast, is transmitted directly from the olfactory bulb, the first olfactory processing center, to the olfactory cortex. This direct link between periphery and higher brain areas makes the olfactory system an interesting model to investigate the transformation of sensory input into a higher neuronal representation.

The Olfactory System

Chemicals in the environment are detected by olfactory sensory neurons in the nasal epithelium. These sensory neurons transform chemical signals into electrical signals. The primary second messenger involved in olfactory signal transduction is cyclic AMP, which is synthesized by adenylyl cyclase upon odorant induced activation of a G protein coupled receptor. Cyclic AMP opens cyclic nucleotide-gated ion channels, which leads to a modest depolarization and Ca^{2+} influx. Ca^{2+} then opens Ca^{2+} - activated chloride channels. Because the reversal potential for chloride is near 0 mV in olfactory sensory neurons, the opening of chloride channels further amplifies the depolarization and constitutes the major amplification step in the signal transduction cascade (Review: Frings, 2001). Alternative signal transduction pathways that may operate in subsets of olfactory sensory neurons involve inositol trisphosphate (Reviews: Restrepo et al, 1996; Schild & Restrepo, 1998). Electrical signals are transmitted to the olfactory bulb (OB) where sensory neurons converge onto OB principal cells in structures termed glomeruli.

A variety of interneuron classes, a subset of which receives direct input from sensory neurons, mediates the interaction between neurons within and across (neighboring) glomeruli and thereby dynamically shapes the output of the OB (Reviews: Lledo et al, 2008; Mori et al, 1999). Axons of mitral and tufted cells, the principal neurons in the OB, form the olfactory tracts that project to multiple central targets including anterior olfactory cortex, piriform cortex, entorhinal cortex, olfactory tubercle, amygdala, and agranular insula (Finger, 1975; Levine & Dethier, 1985; Neville & Haberly, 2004; Rink & Wullimann, 2004; von Bartheld et al, 1984; Wilson et al, 2006).

In the piriform cortex, a major target of the OB in mammals, mitral cells project to broad and overlapping terminal patches (Buonviso et al, 1991; Ojima et al, 1984). Afferent activity is then processed by an extensive associational network of excitatory pyramidal cells and inhibitory interneurons (Neville & Haberly, 2004). Individual pyramidal cells contact a large number (> 1000) of additional pyramidal cells distributed throughout very large areas within piriform cortex (Johnson et al, 2000). Diverse neuromodulatory inputs differentially influence afferent and associational connections (Hasselmo & Bower, 1992; Tang & Hasselmo, 1994).

Representation of odorants in the olfactory bulb (OB)

In the vertebrate OB odorants are represented by combinatorial and chemotopic patterns of activity across glomeruli (Friedrich & Korsching, 1997; Friedrich & Korsching, 1998; Mori et al, 2006; Uchida et al, 2000; Xu et al, 2000). Each glomerulus receives direct input from only one type of olfactory sensory neuron expressing one type of odorant receptor (Malnic et al, 1999), and sensory neurons expressing the same odorant receptor converge onto only one or a few glomeruli (Mombaerts et al, 1996; Ressler et al, 1994; Vassar et al, 1994). Odor stimuli are therefore represented by discrete combinations of activated glomeruli. Glomeruli receiving inputs from chemically distinct classes of molecules are topographically segregated. Thus,

the OB contains a chemotopic map of sensory features. This map is hierarchically organized: Primary molecular features, such as defined functional groups, are mapped onto relatively large regions, whereas secondary features, for example chain length, are mapped within these regions in a more overlapping fashion (Friedrich & Korsching, 1997; Friedrich & Korsching, 1998; Mori et al, 2006; Uchida et al, 2000).

The topographical organization of sensory inputs is largely preserved in the activity patterns of mitral cells and thus at the output level of the OB. Mitral cells responding to different stimulus classes (e.g. amino acids and bile acids) are clearly segregated and the majority of mitral cells responds selectively to only one stimulus class (Yaksi et al, 2009).

Representation of odorants in higher brain areas

In the piriform cortex, pyramidal cells responsive to different stimulus classes are distributed and intermingled (Illig & Haberly, 2003; Rennaker et al, 2007; Zou et al, 2005) and individual neurons respond to molecularly diverse odorants (Kadohisa & Wilson, 2006; Wilson, 2003; Yoshida & Mori, 2007). However, the nature of odor representations in piriform cortex is still poorly understood. Moreover, the mechanisms that determine the integration of odor-evoked activity in individual higher-order neurons of vertebrates remain to be explored.

In the mushroom body, a higher olfactory brain area of insects, Kenyon cells, the mushroom body intrinsic neurons, receive convergent inputs from multiple antennal lobe projection neurons and odorants are represented by sparse patterns of activity across Kenyon cells (Laurent & Naraghi, 1994; Perez-Orive et al, 2002). This sparsening is the result of intrinsic neuronal and circuit properties in the insect olfactory system (Review: Laurent, 2002).

Synthetic perception of odorant mixtures

Animals and humans perceive complex odorant mixtures not as a discernible combination of their components but as novel odor objects (Jinks & Laing, 2001; Staubli et al, 1987). However, little is known about the information processing strategies underlying this transformation of discrete inputs into a coherent odor percept. At the output level of the OB, responses to binary mixtures are often dominated by one of the component responses (Giraudet et al, 2002; Tabor et al, 2004), indicating that odor representations in the OB retain much, albeit not all, information about the components. The creation of mixture-specific representations may therefore occur primarily at higher processing stages and depend on the strategies used by higher-order neurons to extract information from the OB output.

In an extreme case, higher-order neurons might summate converging inputs and fire upon reaching threshold. The response selectivity would then depend strongly on the firing threshold, and mixture responses could be predicted from the component responses by a relatively simple algorithm. Alternatively, more sophisticated integration strategies could enable neurons to detect specific patterns of input activity. Neurons responding to binary odor mixtures but not their individual components have been found in the olfactory cortex by electrophysiological experiments (Yoshida & Mori, 2007) and immediate early gene expression (Zou & Buck, 2006). Responses to multi-component mixtures further suggest that neurons in the olfactory cortex may employ complex strategies to extract information from mitral cell output (Barnes et al, 2008). However, further experiments are required to understand the principles by which mitral cell activity patterns are read out by circuits in higher brain regions. I therefore used binary mixtures to investigate the basic strategies underlying the formation of synthetic mixture representations in a higher brain region.

The relevance of neuronal synchronization in olfactory processing

Information may be encoded in the brain not only by the identity of neurons but also by the temporal patterns of action potentials. While the relative timing of action potentials obviously encodes information in some sensory systems such as the auditory system (Joris & Yin, 2007; Nemenman et al, 2008), its role in other systems remains controversial (Borst & Theunissen, 1999; Oram et al, 2001).

In the first processing center of vertebrate and invertebrate olfactory systems, the olfactory bulb and antennal lobe, respectively, odor stimulation induces a rhythmic synchronization of dynamic and stimulus-specific ensembles of projection neurons that manifests itself in an oscillation in the local field potential (LFP) (Adrian, 1942; Friedrich & Laurent, 2001; Hughes & Mazurowski, 1962; Kashiwadani et al, 1999; Kay & Stopfer, 2006; Laurent, 1996; Laurent, 2002; Laurent & Naraghi, 1994; Rall & Shepherd, 1968; Satou, 1990; Wehr & Laurent, 1996). In locusts and probably in other insects, Kenyon cells in the next processing center, the mushroom body, selectively extract information conveyed by synchronized projection neurons in the antennal lobe by coincidence detection (Laurent & Naraghi, 1994; Perez-Orive et al, 2004; Perez-Orive et al, 2002). In vertebrates, however, it remains unclear whether neurons in target areas of the OB also read synchronized OB output, or whether they integrate synaptic inputs independently of synchronization.

Studies in zebrafish revealed that synchronized and non-synchronized action potential patterns across mitral cells (MCs) convey information about complementary stimulus features (Friedrich et al, 2004). A simple model has demonstrated that information conveyed by synchronized or non-synchronized MC activity patterns could be read out selectively by neurons acting as temporal integrators or coincidence detectors, respectively (Friedrich et al, 2004). It is therefore important to determine how the

integration of synaptic inputs in target areas of the OB depends on their synchronization.

Individual neurons can act as coincidence detectors if they have short membrane time constants (Bernander et al, 1994; Koch et al, 1996) or if they express active conductances that amplify fast transients or inputs arriving at a specific frequency (Desmaisons et al, 1999; Laurent & Naraghi, 1994) (Reviews: Hutcheon & Yarom, 2000; Llinás, 1988). In addition, coincidence detection can be achieved by circuit mechanisms such as delayed feedforward inhibition, which defines a time window for the integration of excitatory inputs (Mittmann et al, 2005; Pouille & Scanziani, 2001; Swadlow, 2003). In Kenyon cells of the insect mushroom body, coincidence detection is achieved by at least two mechanisms: fast transients caused by synchronized projection neuron input are amplified by active dendritic conductances, and phase-delayed feedforward inhibition limits the time window of integration for each oscillatory cycle (Laurent & Naraghi, 1994; Perez-Orive et al, 2004; Perez-Orive et al, 2002). It is unclear, however, whether similar mechanisms also establish coincidence detection in higher-order neurons of the vertebrate olfactory system.

Odor responses recorded in the mammalian olfactory cortex show oscillatory activity that is correlated with stimulus-evoked oscillations in the OB (Bressler, 1987a; Bressler, 1987b) (but see Eeckman & Freeman, 1990). These and further studies indicate that the afferent input to piriform cortex contains an oscillatory temporal structure that is then sustained by intrinsic network mechanisms (Ketchum & Haberly, 1993). Additional investigations in brain slices showed that pyramidal cell responses to olfactory tract stimulation are curtailed by feedforward inhibition (Franks & Isaacson, 2006; Luna & Schoppa, 2008). It is, however, not known whether the odor-evoked rhythmical synchronization of MCs plays a role in shaping the odor selectivity of higher-order neurons. I therefore analyzed the temporal integration

properties of neurons in a higher olfactory brain area and examined their impact on odor responses.

Zebrafish as a vertebrate model in systems neuroscience

A comprehensive understanding of sensory processing by populations of neurons is remarkably facilitated by the use of a small animal model since it allows investigating comparatively large proportions of the entire system. The zebrafish OB contains a relatively small number of glomeruli (100 – 200) and the genome contains only about 143 olfactory receptor genes (Alioto & Ngai, 2005), compared to more than 1800 glomeruli and 1000 olfactory receptor genes in the mouse (Zhang & Firestein, 2002). Moreover, the OB and higher olfactory forebrain areas of zebrafish are much smaller and contain a lower number of neurons than homologous brain areas in mammals, making them accessible to optical imaging approaches. Nevertheless, the major organizational principles of the olfactory system are conserved across species (Ache & Young, 2005; Sato et al, 2007). The zebrafish therefore exhibits important advantages that make it an attractive vertebrate model in systems neuroscience.

In the last decades investigations in an explant preparation of the adult zebrafish brain and nose have provided significant insight into the processing of odorants at the periphery and in the OB (Reviews: Friedrich et al, 2009; Korsching, 2005; Korsching, 2001), providing an excellent basis for studies of olfactory processing in higher brain areas. For the present investigations I focused on the dorsal posterior telencephalon (Dp), a direct target area of the OB that is homologous to the mammalian olfactory cortex (Wullimann & Mueller, 2004).

Aim of this study

The principles by which activity patterns across mitral cells are processed in higher brain areas depend on the integration of inputs by downstream neurons. To investigate the integration of olfactory bulb output by neuronal circuits in the zebrafish telencephalon I focused on two major questions:

Circuit mechanisms shaping odor responses in the dorsal posterior telencephalon (Dp)

I used 2-photon Ca^{2+}- imaging of neuronal activity patterns to quantify responses of Dp neurons to individual compounds and their binary mixtures. The results show that, unlike MCs, Dp neurons exhibited pronounced mixture interactions and frequently showed selective responses to either the mixture or the components. I further investigated the mechanistic basis underlying the observed mixture interactions by pharmacological experiments and whole-cell patch-clamp recordings. I found that GABAergic inhibition played a major role in shaping the odor responses of Dp neurons, and that odor-evoked spiking was controlled by a balance of excitatory and inhibitory mechanisms. These mechanisms endow Dp neurons with the ability to detect specific patterns of activity and inactivity across the population of MCs.

Temporal integration in Dp

I investigated the temporal characteristics of the neuronal circuitry in Dp by measuring biophysical properties and odor responses of higher-order neurons within the intact network. The temporal structure of odor responses was analyzed along with the simultaneously recorded local field potential in the OB. Responses of Dp neurons were not restricted to synchronous oscillatory activity but reflected the integration of inputs over time. Thus Dp neurons may extract information from non-synchronized MC spikes carrying information about the identity of odorants.

MATERIALS AND METHODS

Brain explant preparation

Zebrafish (*Danio rerio*) were kept at 26-27°C on a 13/11-h light/dark cycle following standard procedures. Experiments were performed in an explant preparation of the intact adult (> 3 months old) zebrafish brain and nose as described (Friedrich & Laurent, 2001; Tabor et al, 2004). Briefly, fish were anesthetized by cooling, decapitated in teleost artificial cerebral spinal fluid (ACSF) (Mathieson & Maler, 1988), and the ventral forebrain was exposed. After removal of the dura mater, the preparation was placed ventral-side up into a custom-made flow chamber and continuously superfused with ACSF. Experiments were performed at room temperature (~ 22ºC). All animal procedures were conducted in accordance with official animal care guidelines and approved by the Federal Republic of Germany and the Veterinary Department of the Canton of Basel-Stadt (Switzerland).

Odor stimulation

Amino acids and bile acids – of the highest available purity (Fluka; Neu-Ulm, Germany or Sigma Aldrich; Munich, Germany) – were used for odorant stimulation. Amino acids and bile acids are present in the natural aquatic environment (Carr, 1988; Hara, 1994) and therefore represent realistic olfactory stimuli for fish. Fresh solutions (amino acids 10 μM; bile acids 1 μM) were prepared from frozen stocks (10 or 1 mM, respectively) prior to each experiment. These concentrations are in the intermediate physiological range (Carr, 1988), do not saturate glomerular responses (Friedrich & Korsching, 1997; Friedrich & Korsching, 1998), and had been used in previous experiments. Amino acids and bile acids evoke responses of similar magnitude at these concentrations. In a subset of experiments, 10-fold higher stimulus concentrations were used, but no obvious differences were observed.

Data were therefore pooled. Food extract was prepared from scientific fish food (SDS-400; Special Diets Services, Witham, Essex, UK) as previously described (Tabor et al, 2004). Briefly, a stock solution was prepared by suspending 200 mg of dry food in 50 ml of ACSF and leaving it on the shaker at 4ºC for 2-3 hours prior to filtering. Stock solution was stored at 4ºC and diluted 1:100 in ACSF immediately before the experiment.

Odorants were delivered through a constant flow directed at the nares using a computer-controlled, pneumatically actuated HPLC injection valve (Rheodyne, Rohnert Park, CA) as described (Tabor et al, 2004). Odor applications were separated by at least 90 s to avoid sensory adaptation.

Ca^{2+}- imaging

Odor-evoked Ca2+ signals in somata of Dp neurons were measured by 2-photon microscopy following similar procedures as described for the OB (Yaksi & Friedrich, 2006; Yaksi et al, 2007). Briefly, 50 µg of rhod-2-AM were dissolved in 16 µl of DMSO/Pluronic F-127 (80/20; Invitrogen/ Molecular Probes), diluted 1:10 in ACSF and pressure-injected into Dp using a broken-tip patch-pipette with a tip diameter of approximately 1 – 2 µm. Two to three injections were needed to load the entire Dp. Measurements started at least 60 min after the last injection. Ca2+ signals were detected using a custom-built multiphoton microscope equipped with a 20 × water immersion objective (NA, 0.95; Olympus or NA, 1.0; Zeiss). Two-photon fluorescence was excited at 840 nm by a mode-locked Ti:Sapphire laser (100 fs; 80 MHz; SpectraPhysics, Mountain View, CA). Fluorescence emission was detected externally by a photomultiplier-based whole-field detector through an emission filter (610/75nm). Laser intensity was optimized to minimize noise and photobleaching. Images were acquired at 8 Hz at a resolution of 256 × 128 pixels/frame with custom-written software (ScanImage; Svoboda Lab, Cold

Spring Harbor Laboratory and Janelia Farm Research Campus (see Pologruto et al, 2003)). Two to four trials were averaged for each odor stimulus.

Electrophysiology

Dp neurons were visualized by differential interference contrast (DIC) or similar optics and contrast-enhanced video display. Intracellular recordings were performed with borosilicate pipettes (9 – 15 MOhm). Signals were amplified (Axoclamp 2B or MultiClamp 700B; Axon Instruments/Molecular Devices), filtered at 4 kHz, and digitized at 10 kHz using National Instruments hardware. Odor responses were recorded in whole-cell current-clamp. Intracellular solution contained (in mM) 130 K-gluconate, 10 Na-gluconate, 10 Na-phosphocreatine, 4 NaCl, 4 Mg-ATP, 0.3 Na-GTP, 10 HEPES; pH adjusted to 7.25 with KOH; osmolarity adjusted to ~300 mOsm with K-gluconate.

Local field potential recordings were performed with low resistance patch-pipettes filled with ACSF (4 – 7 MOhms). Field potentials were measured in the center of the ipsilateral OB approximately 150-200 μm below the surface using a MultiClamp 700B amplifier and band-pass filtered (5 – 40 Hz) after acquisition.

Data were acquired and analyzed using custom software written in IgorPro (Wavemetrics) or Matlab (MathWorks, Inc.).

Simulation of input to Dp neurons

For the simulation of odor-evoked MC inputs impinging onto Dp neurons I generated spike trains with varying degrees of synchronization at a carrier frequency of 20 Hz (**Fig. 10**). For each simulated presynaptic cell spikes were generated randomly from probability functions (p) with variable index of synchronization (s) according to:

$$p = s \times \sin(20 \times 2\pi \times t) + 1 \text{ for } s \leq 1$$
$$p = (\sin(20 \times 2\pi \times t) + 1)^S \text{ for } s > 1$$

where t is time in seconds. Probability functions were normalized to the mean. Spike times falling in the refractory period of a previously generated spike were deleted and drawn again from the same probability distribution. Spike trains generated with the same probability function were summed for all presynaptic cells and convolved with a postsynaptic current waveform (PSC). The shape of the PSC was modelled by an alpha function, which is defined by an exponential rise and an exponential decay. Table 1 shows parameters chosen for the presynaptic population activity (number of presynaptic cells, time-averaged spike frequency for each cell, absolute refractory period) and the postsynaptic current elicited by each spike (rise and decay times of the PSC). Low synchronization indices s produced flat probability functions, resulting in nearly Poisson-distributed spike times. Increasing the synchronization index created spike trains with increasing degrees of synchronization at an oscillatory frequency of 20 Hz, which corresponds to the frequency of odor-evoked LFP oscillations in the zebrafish OB (Friedrich et al, 2004; Friedrich & Laurent, 2001; Tabor et al, 2008).

Parameter	**Chosen value**
Number of presynaptic cells	20
Time-averaged spike frequency of each cell	20 Hz
Absolute refractory period	5 ms
Rise time constant of PSC	0.8 ms
Decay time constant of PSC	5 ms

Table 1: Parameters for the simulation of artificial input currents

PSC: Postsynaptic current in response to one presynaptic spike.

Data Analysis

Imaging

Series of fluorescence images were converted into image series depicting the relative change in fluorescence (ΔF/F) in each pixel. The baseline fluorescence F was determined by averaging raw images over two seconds before stimulus onset. Response maps were constructed by averaging ΔF/F frames over a period of 3 seconds after response onset. Data were not corrected for bleaching since the effect was negligible. In the ΔF/F images, neuronal somata were outlined manually and the response of each soma to each stimulus was determined. Neurons that did not respond to any stimulus were excluded from further analyses. A control analysis demonstrated that mixture interactions did not depend on the sequence of stimulus application, confirming that the observed effects cannot be explained by non-stationary responses.

The mean coefficient of variation, CV_{rep}, was determined from two repeated applications of the same odor stimulus. Repeated stimulus applications were separated in time by approximately 40 min. Only neurons with a mean response exceeding at least three times the detection threshold were included in the calculation of CV_{rep}, as in other analyses.

Electrophysiology

Average values are given as mean ± standard deviation. For the analysis of the dual channel recordings of OB local field potential (LFP) and Dp neuron membrane potential the recorded traces were normalized to the respective standard deviation in a 2 s window prior to stimulus onset. From this normalized data, power spectral densities (PSDs) were calculated over 2 s time windows before and during odor stimulation. PSDs were then averaged over repeated trials with each cell-odor pair. The average peak oscillation frequency of the LFP was 14.7 ± 4.6 (range: 7.3 Hz to 27.5 Hz; n = 66 cell-odor pairs). The mean oscillation power in the LFP and the membrane

potential of a simultaneously recorded Dp neuron was then calculated by averaging the power in a frequency band of 3.6 Hz around the peak oscillation frequency for each cell-odor pair.

To quantify subthreshold membrane potential changes voltage traces were median filtered using a sliding window of 14 ms. Slow membrane potential changes were further isolated by 5 Hz low-pass filtering. The maximum depolarization within 5 s around the stimulation period was then quantified by averaging the membrane potential in a 100 ms time window centered on the maximum value and subtracting the resting membrane potential. The low-pass filtered trace was subtracted from the median filtered membrane potential trace to isolate fast subthreshold components. This trace was then 5 – 40 Hz band-pass filtered prior to determining the amplitudes of oscillatory membrane potential fluctuations during the LFP oscillation period (2 s). Maximum fluctuations were calculated for each cell-odor pair by averaging the largest 10 % of fluctuations.

RESULTS

Circuit mechanisms shaping odor responses in Dp

Responses to binary mixtures analyzed by 2-photon Ca^{2+} - imaging

For the investigation of sensory processing in a higher olfactory brain area I used a nose-attached explant preparation of the intact adult zebrafish brain. Odor responses in the dorsal posterior telencephalon (Dp) were imaged at single-neuron resolution using 2-photon microscopy (Denk et al, 1990) after bolus loading of a Ca^{2+} - sensitive dye (Stosiek et al, 2003) and quantified by the relative change in fluorescence (ΔF/F). Odor responses in Dp were reproducible and stimulus-specific (**Fig. 1**).

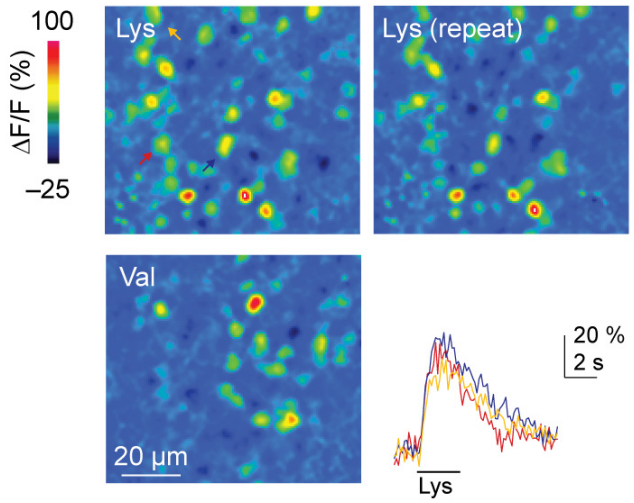

Figure 1: Odor responses in Dp.

Ca^{2+} signals evoked in Dp by odor stimulation (single trials). Response magnitudes are color-coded. Response maps are reproducible (Lys versus Lys repeat) and stimulus-dependent (Lys versus Val). Traces show time course of Ca^{2+} signals in the somata indicated by arrows.

To examine the mechanisms by which Dp integrates sensory inputs I measured the responses of multiple Dp neurons to amino acids and bile acids. Amino acids and bile acids stimulate segregated glomeruli in the lateral and medial OB, respectively, and MC activity patterns for amino acids with different secondary molecular features do not overlap (Friedrich & Korsching, 1997; Friedrich & Korsching, 1998). Somatic Ca^{2+} signals were obtained for a total of 240 neuron-mixture pairs in five fish.

As odor stimuli I used individual compounds and binary mixtures. The individual stimuli comprised one bile acid (taurodeoxycholic acid, TDCA) and three amino acids. Two of the amino acids (Tyrosine, Tyr; and Tryptophan, Trp) shared the same secondary molecular feature (aromatic side chain), while the third (Arginine, Arg) had a different secondary molecular structure (basic side chain) (**Fig. 2**). Mixtures were either composed of two amino acids (usually 10 µM each) or of one amino acid (10 µM) and TDCA (1 µM).

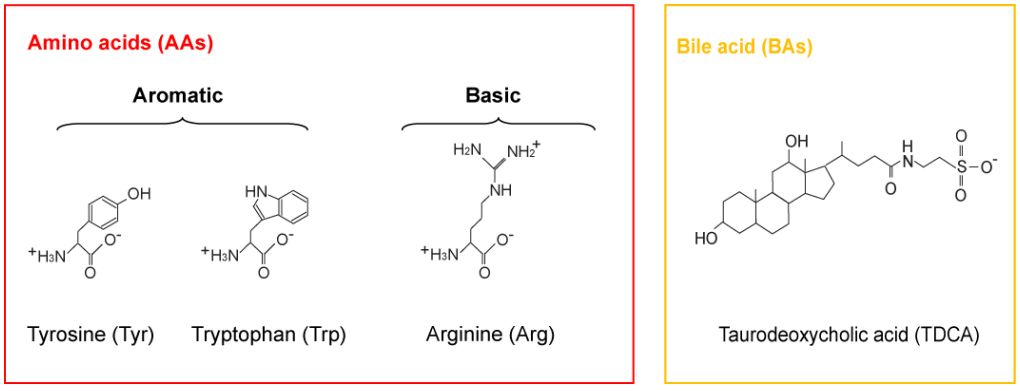

Figure 2: Chemical structures of individual odor stimuli used for binary mixture experiments.

For each neuron-mixture pair I determined whether the neuron responded to at least one of the individual components, to their binary mixture, or to both. I counted a response if the evoked Ca^{2+} signal exceeded a detection threshold defined as two times the SD of the Ca^{2+} signal in trials without odor. To avoid artifacts resulting from signals close to the detection threshold, neuron-mixture pairs were included in the analysis only when at least one of the three responses (either component or the mixture) exceeded three times the detection threshold.

Individual neurons responded frequently in a mixture- or component-selective fashion (20 % of the neuron-mixture pairs). Surprisingly, component-selective responses were more frequently observed than mixture-selective responses (**Fig. 3B, left**). Hence, interactions between components in a mixture appear to be prominent in Dp.

I next examined the relationship between mixture and component responses by not only counting responses in an all-or-non fashion but by determining the relative response magnitudes. The similarity of the mixture response to the component responses was determined by mapping the magnitude of the mixture response of each neuron-odor pair onto the interval between the component responses such that the smaller component response is represented by a value of zero and the larger component response is represented by one. The magnitude of the mixture response often fell in between the component responses (**Fig. 3B, center**). Mixture responses were therefore not dominated by one of the two component responses. This is clearly different from mixture responses in the OB where MCs usually exhibit a clear "component dominance" (Giraudet et al, 2002; Tabor et al, 2004; Yaksi et al, 2009).

I further investigated mixture interactions by quantifying mixture suppression and mixture synergism. Mixture synergism was defined as a response to the mixture that is greater than the larger component response,

multiplied by a safety factor. This safety factor was introduced to minimize false positives caused by the natural response variability. It was defined as 1 + CV_{rep}, where CV_{rep} is the mean coefficient of variation of responses to repeated applications of the same stimulus (see Materials and Methods). Mixture suppression was defined accordingly as a response to the mixture that is smaller than the larger component response, multiplied by a safety factor defined as 1 – CV_{rep}. Many mixture responses (44 %) showed suppression, but synergism also occurred relatively frequently (17%) (**Fig. 3B, right**). 11 % of the mixture responses exhibited strong mixture synergism: they were larger than the sum of both component responses multiplied by the safety factor, 1 + CV_{rep} (**Fig. 3B, right, narrow bar**).

These results confirm that odor responses of Dp neurons are shaped by complex mixture interactions and indicate that mixture suppression is particularly prominent.

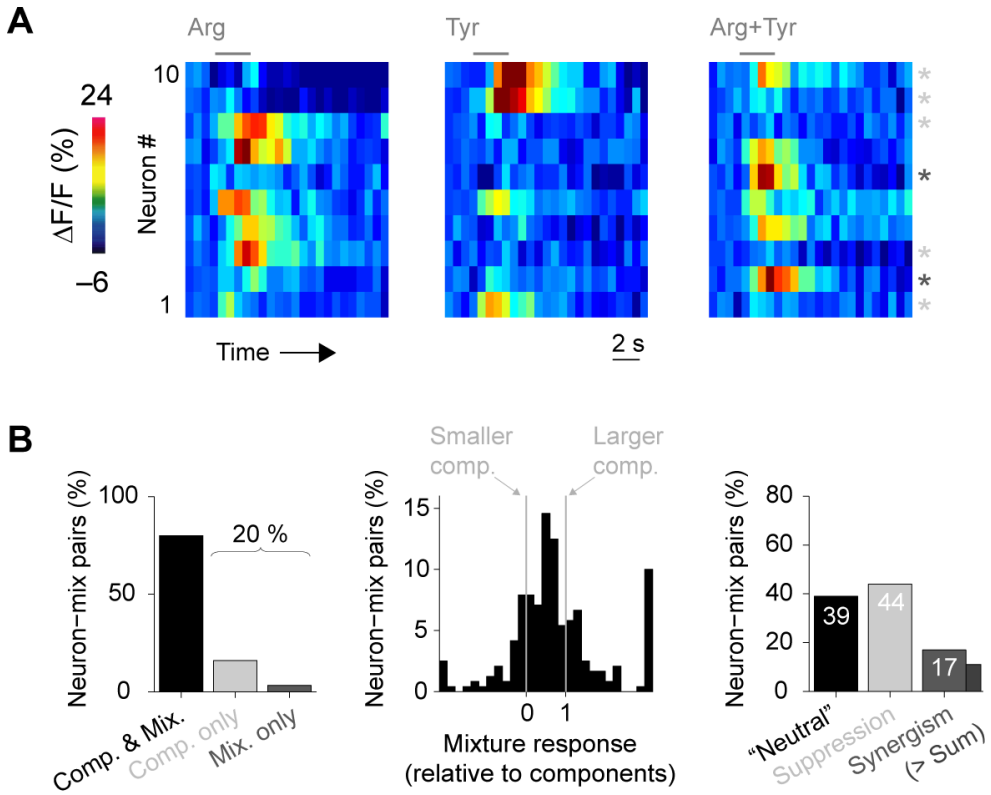

Figure 3: Mixture interactions in Dp.

(A) Responses of 10 simultaneously imaged Dp neurons to two individual odorants and their binary mixture. For each neuron, ΔF/F is plotted against time. Odor stimulation periods are indicated by gray bars. Light and dark stars depict mixture suppression and mixture synergism, respectively.

(B) Left: Percentage of neuron-mixture pairs that responded to the mixture and at least one component (Comp. & Mix.), to one or both components only (Comp. only), and to the mixture only (Mix. only). Center: histogram of mixture response magnitudes relative to component responses. Response magnitudes were scaled so that the smaller component response equals 0 and the larger component response equals 1. Right: Frequency of neutral mixture responses, suppression and synergism. Numbers indicate percentages. Narrow bar on the right (> Sum) indicates percentage of mixture responses larger than the sum of the component responses multiplied by the safety factor, $1 + CV_{rep}$.

Given the chemotopic representation of odorants at the level of the OB, I was interested whether the pronounced mixture interactions observed in Dp depend on the spatial segregation of activated MCs. Since amino acids and bile acids activate segregated areas in the OB, I separately analyzed the responses to mixtures of two amino acids (n = 133 neuron-mixture pairs) and mixtures of one amino acid and one bile acid (n = 107). The frequency of mixture- or component- selective responses, the distribution of relative response magnitudes, and the occurrence of suppression and synergism were similar, independently of the primary molecular features of the components (**Fig. 4**). To further explore whether mixture interactions in Dp are influenced by the overlap of MC activity patterns, I tested whether mixture interactions differ in response to mixtures of amino acids with the same secondary molecular features (Tyr-Trp, both aromatic; n = 55 neuron-mixture pairs) and mixtures of amino acids with different secondary molecular features (Tyr-Arg, aromatic and basic; n = 78). The frequency of mixture- or component-specific responses and the distribution of relative response magnitudes were similar for Tyr-Trp and Tyr-Arg mixtures (**Fig. 5**). In summary, mixture interactions in Dp show little, if any, dependence on odor classes, indicating that they are not strongly influenced by the locations of MCs in the OB. Consequently, Dp neurons associate inputs from MCs that convey information about different molecular features. Dp therefore has the capacity to integrate information about different molecular components of an odor.

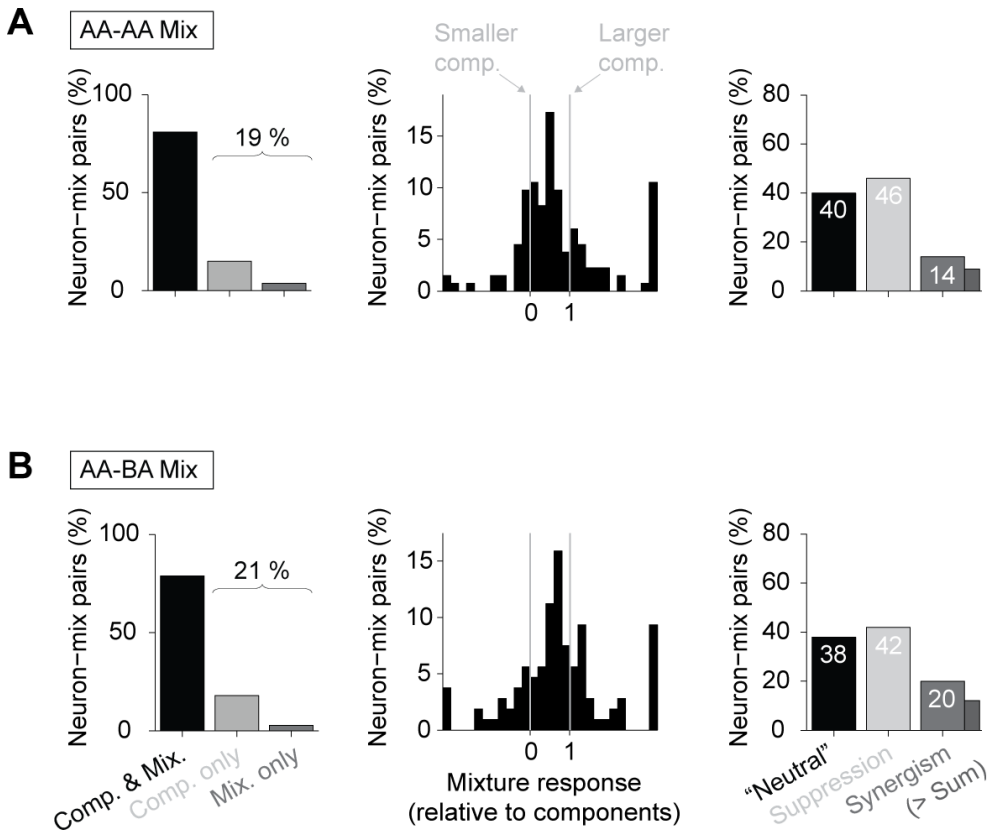

Figure 4: Mixture interactions for responses of Dp neurons to odorants with distinct primary molecular features.

(A) Amino acid – Amino acid mixtures.

(B) Amino acid – Bile acid mixtures.

Conventions are the same as in Fig. 3B.

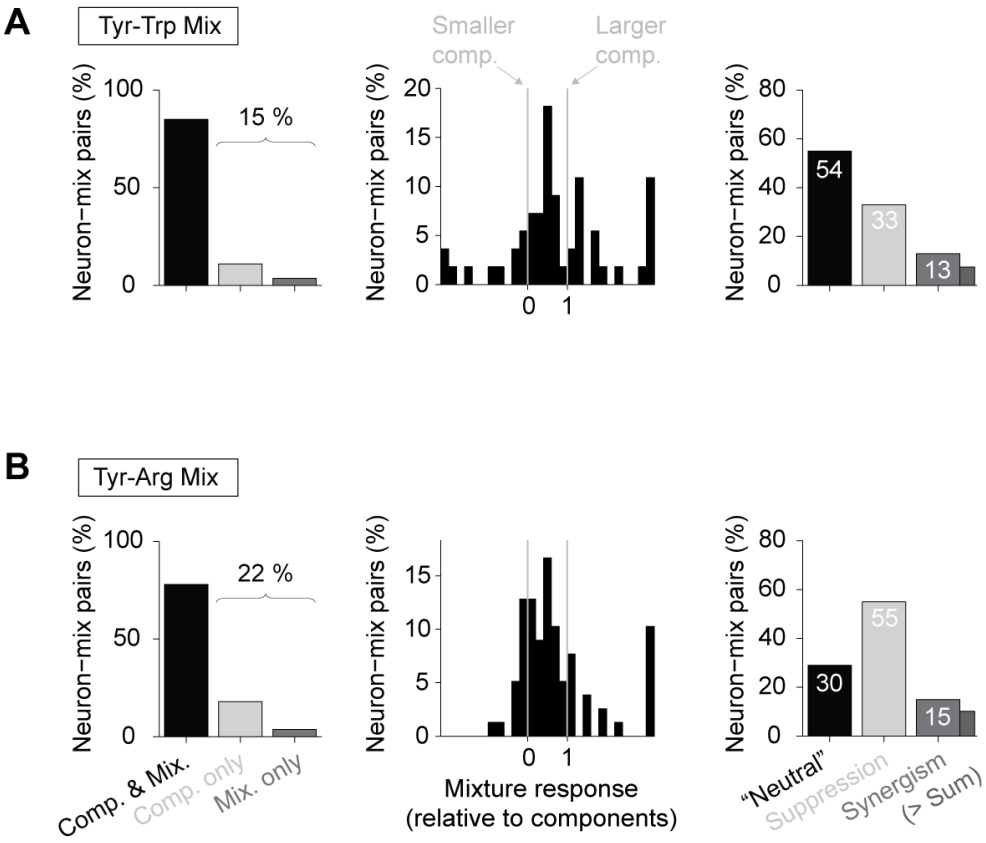

Figure 5: Mixture interactions for responses of Dp neurons to odorants with distinct secondary molecular features.

(A) Mixture of two amino acids with aromatic side chain.

(B) Mixture of one amino acid with aromatic and one with basic side chain.

Conventions are the same as in Fig. 3B.

Mechanistic basis for mixture interactions in Dp

The frequent occurrence of mixture suppression suggests that odor responses of Dp neurons are controlled not only by excitatory inputs but also by inhibitory synaptic pathways. To test this hypothesis, I first injected Gabazine into Dp. Gabazine is a selective $GABA_A$ receptor antagonist that acts by competitive allosteric modulation of channel opening (Ueno et al, 1997). Focal application of Gabazine strongly and reversibly amplified odor-evoked Ca^{2+} signals. The magnitude of odor responses was increased in all experiments (n = 4 fish; **Fig. 6A**). Gabazine injection also modified the time course of odor responses (**Fig. 6B**). In some experiments, the response was slighly prolonged (**Fig. 6B1**), while in others, Gabazine converted a transient response into a more sustained response (**Fig. 6B2**). This demonstrates that odor responses in Dp are under inhibitory GABAergic control.

I further examined the synaptic mechanisms underlying odor responses in Dp by whole-cell patch-clamp recordings (n = 115 neuron-odor pairs in 32 neurons of 17 fish; usually 5 repetitions of each stimulus). In the absence of odors, most Dp neurons were silent or fired spontaneous action potentials at very low rates. For the quantification of odor responses subthreshold responses were counted when the mean membrane potential within at least five consecutive 100 ms time bins during odor stimulation was significantly different from baseline ($P < 0.01$, Wilcoxon rank sum test). Suprathreshold responses were identified as significant changes in firing rate using the same procedure after convolving individual action potentials with a Gaussian ($\sigma = 25$ ms; other values yielded similar results). Upon odor stimulation, subthreshold responses were detected in 93 % of the recorded neuron-odor pairs (**Fig. 7**). The membrane potential response was usually a transient depolarization (70 % of neuron-odor pairs), but hyperpolarizing (10 %) or multiphasic responses (13 %) were also observed (**Fig. 7A**). Despite this broad subthreshold tuning, action potential firing occurred only in 16 % of

the neuron-odor pairs. The firing pattern was usually a short burst (see **Fig. 7A, cell 23**), consistent with the kinetics of Ca^{2+} signals (**Fig. 1 and Fig. 3A**). These results indicate that neurons in Dp receive direct or indirect synaptic input from functionally diverse sets of MCs but respond with action potentials only to specific patterns of input activity.

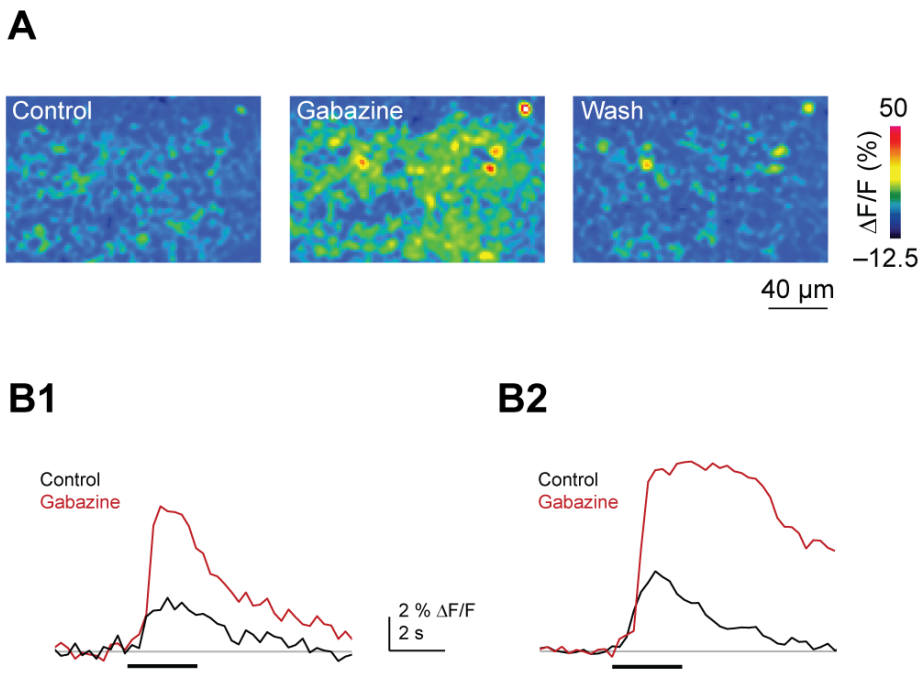

Figure 6: Effect of Gabazine on odor responses in Dp.

(A) Effect on the response magnitude. Ca^{2+} signals evoked by odor stimulation (Arg + TDCA) in Dp before (Control), during (Gabazine) and five minutes after (Wash) pressure injection of Gabazine into the intercellular space (single trials, low magnification).

(B) Effects on the time course. (B1) Time course of odor-evoked Ca^{2+} signal averaged over the entire field of view before and during application of Gabazine for the experiment shown in (A). (B2) Time course of spatially averaged Ca^{2+} signal before and during application of Gabazine in another experiment.

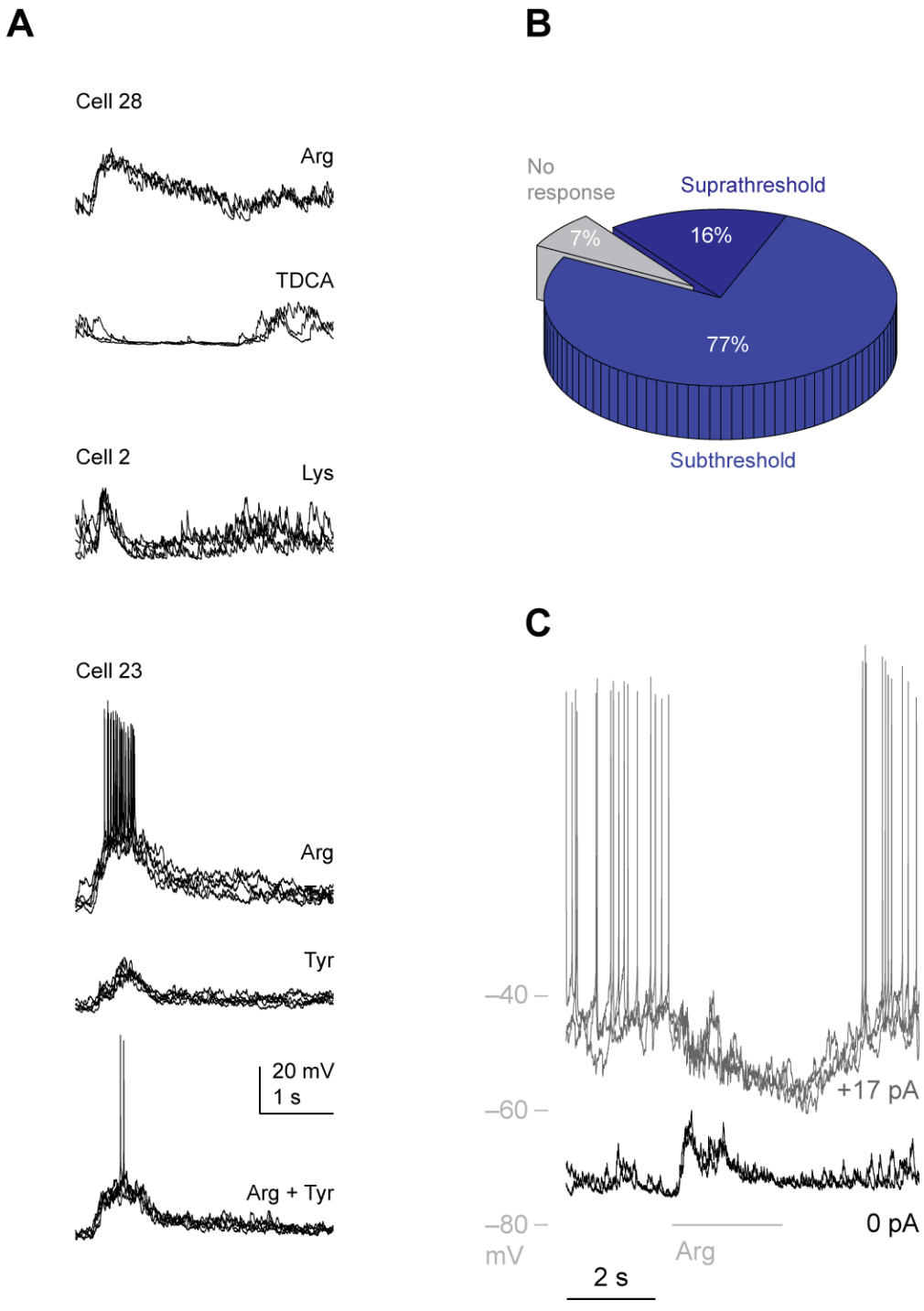

Figure 7: (Legend see next page)

Figure 7: Intracellular current-clamp recordings of odor responses.
(A) Whole-cell recordings of odor responses in Dp neurons. Multiple trials are overlaid for each recording. Stimuli are indicated above the respective traces.
(B) Frequency of response types in Dp.
(C) Response of a Dp neuron to odor stimulation (Arg) at rest (black) and during depolarizing current injection (17 pA; gray).

To reveal the mechanisms controlling action potential initiation, I measured responses to odors that evoked a subthreshold depolarization again during the injection of a depolarizing current. The magnitude of the current was chosen to cause spontaneous action potential firing. In all cases (n = 19 neuron-odor pairs), depolarization resulted in a reversal of the subthreshold response and in the inhibition of action potential firing (**Fig. 7C**). Hence, synaptic input during the odor response drives the membrane potential towards a reversal potential near spike threshold that is, most likely, determined by a mixture of excitatory and inhibitory conductances. The kinetics of the membrane potential responses in the absence and in the presence of current injection were usually not mirror symmetric (**Fig. 7C**), indicating that changes in different conductances follow different time courses. These data indicate that action potential firing in Dp is dynamically controlled by the balance of excitatory and inhibitory inputs, which in turn is determined by the activity pattern across the population of mitral cells.

Temporal integration of synaptic inputs by individual neurons

For the investigation of temporal properties of Dp neurons I performed whole-cell current-clamp recordings from 44 Dp neurons in 31 fish.

In the absence of any injected current, most neurons (79 %) had a resting potential between -60 and -80 mV and spontaneous firing rates smaller than 0.2 Hz. Some neurons (21 %) had slightly more depolarized resting potentials and fired spontaneously at up to 7 Hz. The average input resistance was measured in 16 neurons and found to be 1.1 ± 0.6 GΩ (mean ± SD; range: 0.5 – 2.8 GΩ).

Passive and active properties of Dp neurons

To determine the membrane time constant of Dp neurons, I injected hyperpolarizing and depolarizing current pulses (500 ms or 250 ms) to cause membrane potential changes of approximately 10 to 30 mV (**Fig. 8A**). I quantified the membrane time constant by the decay constant of a single exponential fit to the voltage response recorded during the first 200 ms following stimulus offset (**Fig. 8A**). The calculated time constants were 27.0 ± 10.2 ms (mean ± SD; n = 16 neurons) in response to hyperpolarizing pulses and 46.9 ± 20.8 ms (n = 19 neurons) in response to depolarizing pulses (**Fig. 8B**). The difference between time constants for hyperpolarizing and depolarizing pulses indicates that membrane time constants depend on the membrane potential, presumably because the input resistance is influenced by voltage-gated conductances. However, in all cases, and particularly for depolarizing input currents, the time constant was relatively long in comparison to the oscillation period of synchronized activity in the OB (~ 50 ms). Hence, the passive membrane properties of Dp neurons do not favor the detection of input currents synchronized on a ms time scale.

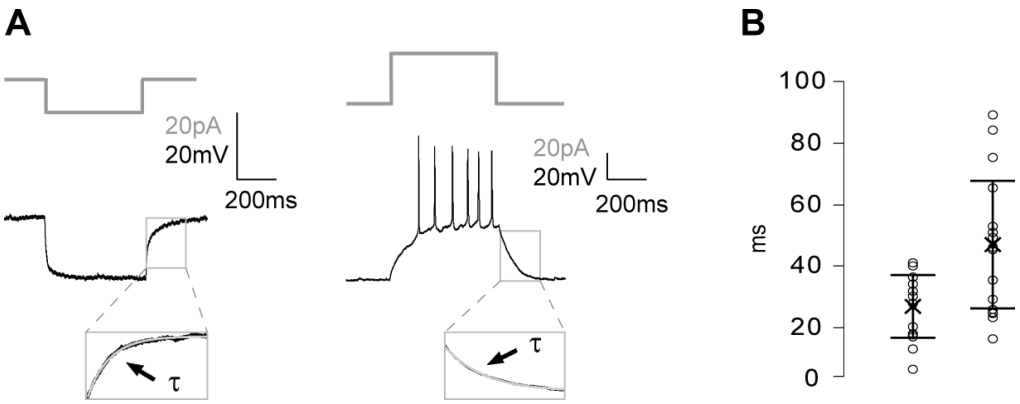

Figure 8: Membrane time constants.

(A) Hyperpolarizing (left) and depolarizing (right) current pulses (gray, top) were applied during whole-cell voltage recordings. Membrane potential responses are shown for two neurons (black, bottom). Time constants were obtained by single exponential fits during 200 ms after pulse offset (insets). (B) Time constant for each cell (open circles) with mean ± SD values for hyperpolarizing (left, n = 16) and depolarizing (right, n = 19) current pulses.

Step depolarizations close to action potential threshold did not evoke membrane potential transients, suggesting that fast inputs are not selectively amplified by active conductances (**Fig. 8A**). To examine this in more detail, I analyzed the frequency-dependence of subthreshold membrane potential changes evoked by sine wave currents of discrete frequencies (3, 10, 20, 30, and 60 Hz; n = 15 neurons) (**Fig. 9A**). The current amplitude was adjusted to evoke membrane potential fluctuations that were near spike threshold at 3 Hz. The frequency-dependence of evoked membrane potential changes was quantified by the impedance (power spectral density of voltage divided by power spectral density of current) (see Hutcheon & Yarom, 2000). In all neurons, the impedance showed no specific frequency tuning but declined

monotonically with increasing frequency, as expected for purely passive filtering by the membrane properties (**Fig. 9C**).

To corroborate this finding, I recorded the membrane potential in response to a 30 s sine wave current with linearly increasing or decreasing frequency ("ZAP" function, see Puil et al, 1986) between 0 and 60 Hz (n = 9 neurons) (**Fig. 9B**). As found with sine waves of constant frequency, the PSD of the membrane voltage decayed constantly with increasing frequency (**Fig. 9D**). These results indicate that individual Dp neurons do not amplify input currents at a particular frequency, but essentially act as passive low-pass filters.

Temporal dynamics of circuit responses

To investigate how input-output functions of Dp neurons in the suprathreshold regime depend on the temporal structure of inputs I simulated trains of postsynaptic currents with different degrees of synchrony (**Fig. 10**). For these artificial input currents I simulated action potentials of 20 individual cells, each firing at a mean frequency of 20 Hz (**Fig. 10B**). I varied the synchrony among action potentials by changing the probability of spiking for each cell from a Poisson distribution to a distribution that peaked at a specific phase during each 50 ms time window (see Materials and Methods) (**Fig. 10A**). The degree of synchrony was defined by the synchronization index, s, that is 0 for random spiking, 1 for a sinusoidal change in firing probability, and >1 for even sharper tuning of spike times. Current commands were then generated by convolving each spike with the waveform of a unitary fast excitatory postsynaptic current (**Fig. 10C,D**) and injected into Dp neurons in whole-cell current-clamp (**Fig. 10E**). Neuronal output was quantified by the spike count. In a small set of neurons (n = 4), the spike output showed no obvious dependence on input synchrony (**Fig. 10E**). Further recordings will be performed to endorse this observation.

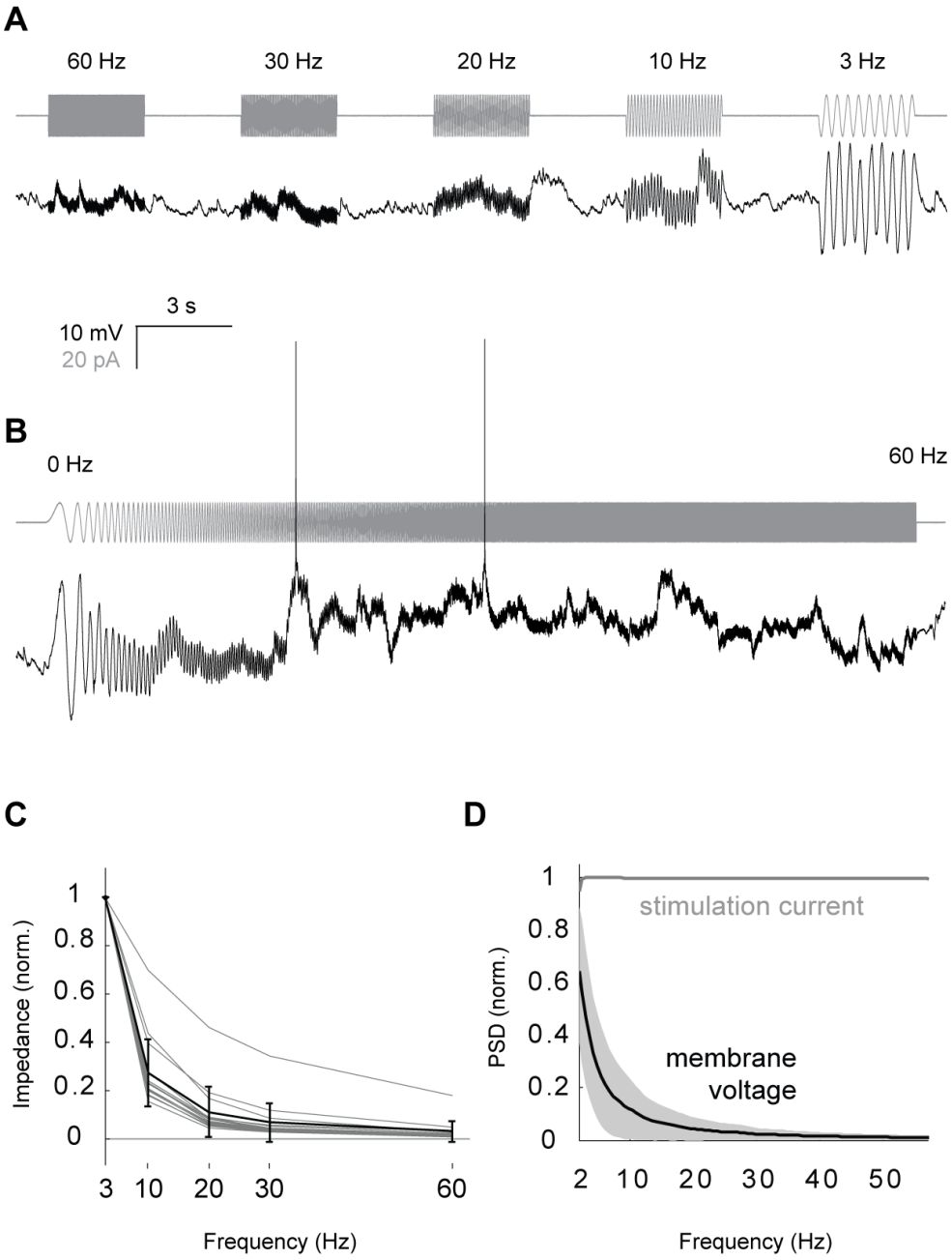

Figure 9: (Legend see next page)

Figure 9: Filter properties.

(A) Whole-cell voltage response of a Dp neuron (black) to sinusoidal currents of different constant frequencies (gray).

(B) Membrane potential of a Dp neuron (black) during injection of a sinusoidal current of linearly increasing frequency from 0 to 60 Hz (gray).

(C) Impedance measured by constant frequency current injections (A), calculated as power spectral density of membrane voltage divided by power spectral density of injected current at each frequency. Gray traces show data obtained for each cell (n = 15 cells) normalized to the impedance at 3 Hz. Black trace shows mean ± SD.

(D) Impedance measured by ZAP current injection (B), shown as mean power spectral densities of voltage responses (black; ± SD; n = 9 cells). The power spectral density of voltage responses is directly proportional to the impedance because the power spectral density of the injected current (gray) is flat.

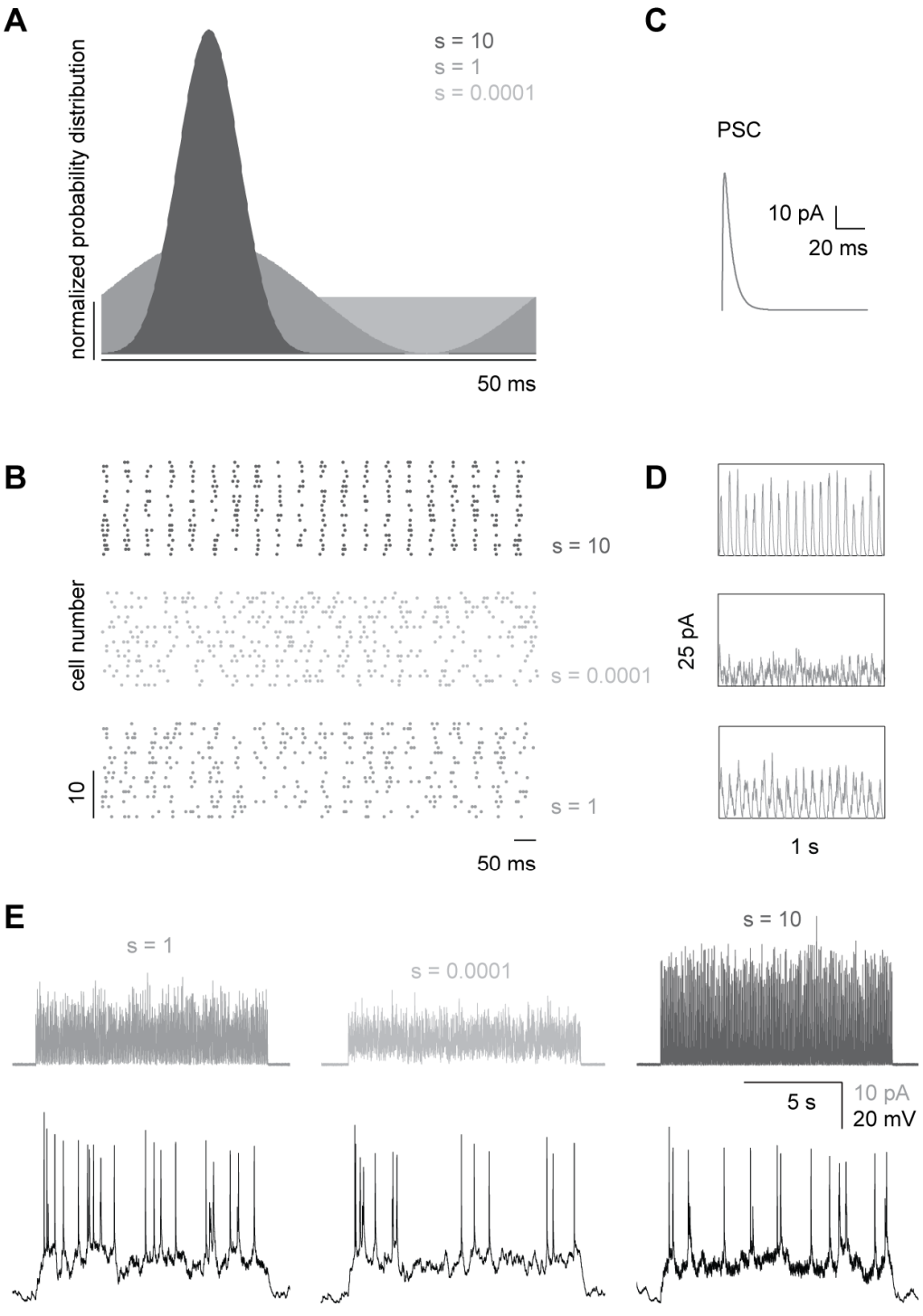

Figure 10: (Legend see next page)

Figure 10: Spike output as a function of input synchrony.
(A) Normalized probability functions giving the probability of spiking during the oscillation cycle (50 ms) for three synchronization indices (low: s = 0.0001; high: s = 1; very high: s = 10).
(B) Raster plots of spike trains generated from the probability functions shown in (A).
(C) Unitary PSC simulating an AMPA receptor current (sum of first-order exponentials; rise time constant 0.8 ms, decay time constant 5 ms, amplitude 60 pA).
(D) Spike trains with the same underlying probability were summed and convolved with the PSC shown in (C). Examples for the obtained currents are shown for each index of synchronization.
(E) Whole-cell current clamp recording from a Dp neuron. Gray: Injected input currents with 3 different degrees of synchrony at 20 Hz: high (left), low (middle) and very high (right). Black: Measured voltage-responses.

Together, my observations indicate that individual Dp neurons are not equipped with passive or active mechanisms that amplify synchronized input or oscillatory input at a frequency near the oscillation frequency in the OB.

Temporal structure of the Dp neuron membrane potentials during odor responses

I next examined the relationship between oscillatory synchronization in the OB and the activity of Dp neurons during odor responses by simultaneous recordings of the LFP in the OB and the membrane potential of Dp neurons (n = 66 neuron-odor pairs; 15 neurons in 8 fish). Odor stimuli included a food extract, five amino acids (arginine, tyrosine, tryptophan, isoleucine, methionine), the bile acid taurodeoxycholic acid (TDCA) and binary mixtures of amino acids or an amino acid and TDCA. Membrane potential responses of Dp neurons usually consisted of a large and slow depolarization and smaller, faster fluctuations (**Fig. 11A**; see also **Fig. 7A,C**). In some recordings, small fluctuations in the membrane potential appeared to be phase-locked to the LFP oscillation (**Fig. 11A**, arrows).

In order to quantitatively compare the temporal structure of LFP oscillations in the OB and membrane potential responses in Dp, each recording was normalized to the standard deviation before response onset. I then first analyzed the power spectral density (PSD) of unfiltered LFP signals and the membrane potential (**Fig. 11B**). Odor stimulation increased the power of the LFP within a clearly defined frequency band between 10 and 30 Hz, consistent with previous results (Friedrich et al, 2004; Friedrich & Laurent, 2001; Tabor et al, 2008). The peak frequency of the LFP oscillation decreased slightly during the odor response (**Fig. 11C**).

To quantify the intensity of oscillatory activity, I measured the power within a 3.6 Hz frequency window centered on the peak frequency of the oscillation during the odor response relative to the power in the same frequency band before response onset. Odor stimulation increased the LFP power in the oscillatory frequency band in all recordings (n = 66) (**Fig. 12**). On average, power increased by a factor of 28.0 ± 47.3 (median: 12.6; range: 1.2 to 274.5). For the membrane potential, the power spectrum was more

complex and often exhibited multiple peaks (**Fig. 11B**). During the odor response, a peak at a frequency corresponding to the LFP oscillation frequency was sometimes observed, but the power generally increased throughout a wide range of frequencies (**Fig. 11B**). The power in the oscillatory frequency band increased in 82 % (54/66) of the recordings and decreased in the remaining 18 % (12/66) in response to odor stimulation (**Fig. 12**). Moreover, the average change in oscillatory power was significantly lower ($p << 0.0001$, Wilcoxon rank sum test) than for LFP recordings (4.8 ± 7.1; median: 2.6; range: 0.03 to 45.7). Hence, oscillatory responses are considerably less pronounced in the membrane potential of Dp neurons than in the LFP in the OB.

The autocorrelation of the normalized LFP showed large-amplitude oscillations with a frequency near 20 Hz (**Fig. 11D**). The autocorrelation of the normalized membrane potential also exhibited periodic fluctuations at a corresponding frequency that were, however, small compared to a much slower component. The cross-correlation of normalized LFP and normalized membrane potential was also oscillatory, but the amplitude was substantially smaller than that of the autocorrelation of the normalized LFP (**Fig. 11D**). Together, these findings demonstrate that synchronized activity of OB output neurons is reflected in the subthreshold membrane potential fluctuations of a subset of Dp neurons, but these fluctuations account only for a small part of the temporal structure in the membrane potential during an odor response.

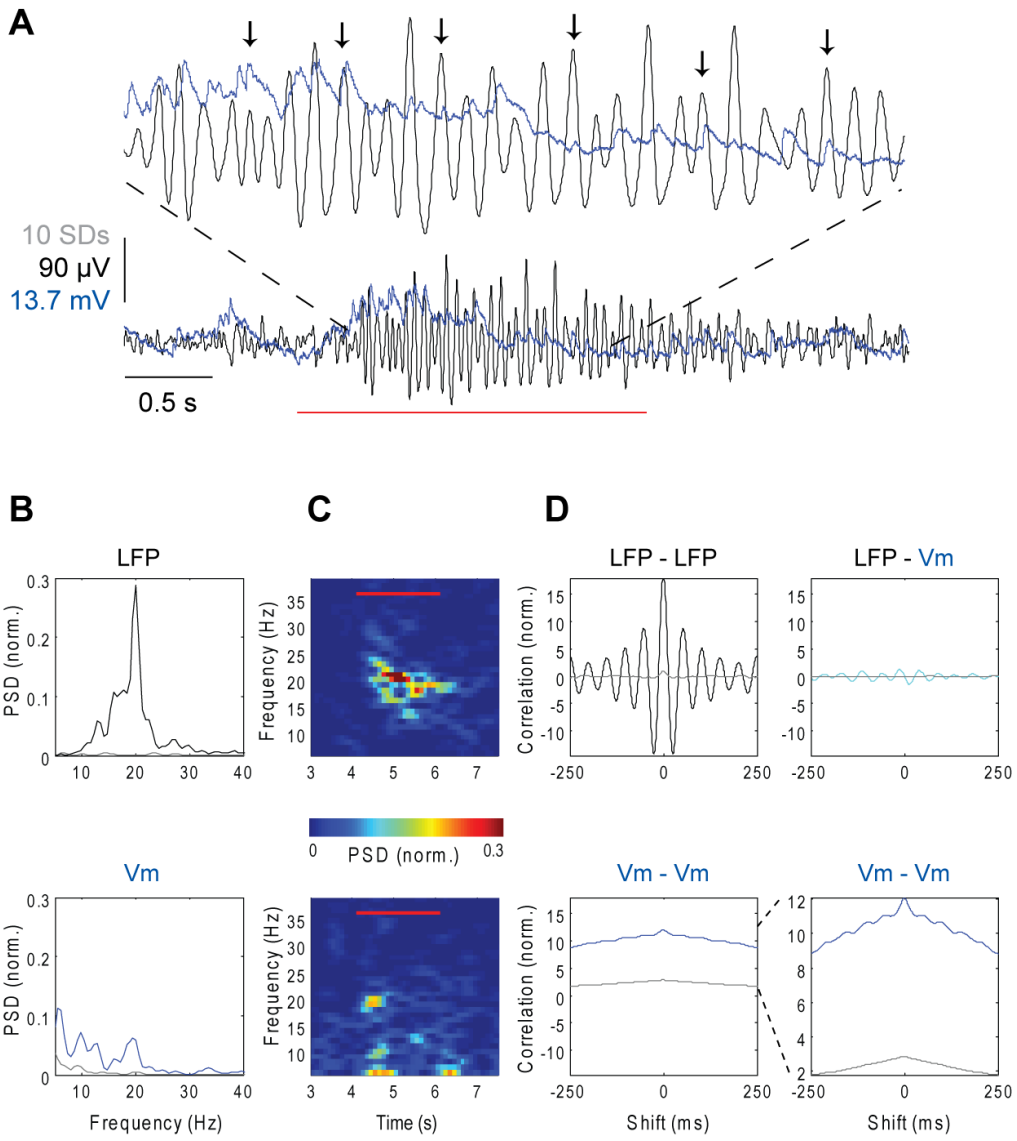

Figure 11: (Legend see next page)

Figure 11: Simultaneous recording of olfactory bulb LFP and Dp neuron membrane potential.
(A) Example of LFP in the OB (black; detrended, 5 – 40 Hz band-pass filtered, normalized to the standard deviation) and simultaneously recorded membrane potential of a Dp neuron (blue; detrended, normalized to the standard deviation) showing prominent subthreshold membrane potential oscillations in response to food extract. Red line indicates 2 s response window for analysis. Inset: Enlargement of a portion of the traces. Arrows depict similarities between fluctuations in the membrane potential and the LFP.
(B) Power spectral densities of LFP (top) and membrane voltage (bottom) for the response window indicated by the red line in (A) (black, blue) and for a 2 s stretch prior to stimulus onset (gray, very close to 0). Traces were unfiltered and normalized in amplitude to the SD before odor stimulation.
(C) Time-resolved frequency content of LFP (top) and membrane voltage (bottom). Red bars indicate the odor stimulation period. Traces were unfiltered and normalized in amplitude to the SD before odor stimulation.
(D) Left: Autocorrelation of normalized LFP (top) and normalized membrane voltage (bottom). Right (bottom): Autocorrelation of normalized membrane voltage; note the different scaling of the y-axis. Right (top): Cross-correlation of normalized LFP and normalized membrane voltage. Black and blue traces for 2 s stretch indicated by red line in (A), gray traces during 2 s stretch prior to stimulus onset.

Role of odor-evoked membrane potential oscillations for spike generation in Dp neurons

In order to estimate the role of synchronized synaptic input on action potential output of Dp neurons I analyzed the contribution of oscillatory membrane potential fluctuations to the overall odor-evoked membrane depolarization. I first extracted the slow membrane depolarization by 5 Hz low-pass filtering of the recorded membrane potential response (**Fig. 13A**, green trace). The residual fast fluctuations (**Fig. 13A**, red trace) were then 5 – 40 Hz band-pass filtered to extract fluctuations corresponding to the LFP oscillation (**Fig. 13A**,

black trace). I then determined the maxima (V_{Osc}) and the peak-to-peak amplitudes (ΔV_{Osc}) (**Fig. 13C, inset**) of the fast fluctuations within a two second time window (**Fig. 13B**) and compared them to the amplitude of the slow component (ΔV_{Slow}). I obtained an average of 40.8 ± 3.5 fluctuations per 2 s time window. The amplitude of the fast fluctuations was determined for each neuron-odor pair either as the mean of the maxima ($V_{Osc, Mean}$) or as the mean of the peak-to-peak amplitudes ($\Delta V_{Osc, Mean}$) of all oscillatory fluctuations. In addition, I quantified the maximum depolarizations induced by the fast fluctuations as the average amplitude of the 10 % largest oscillatory fluctuations for the maximum amplitudes ($V_{Osc, Max}$) or the peak-to-peak amplitudes ($\Delta V_{Osc, Max}$). In all neuron-odor pairs, ΔV_{Slow} was substantially larger than $V_{Osc, Max}$ or $\Delta V_{Osc, Max}$. ΔV_{Slow} amounted to 18.4 ± 9.9 mV, while $V_{Osc, Max}$ and $\Delta V_{Osc, Max}$ amounted to 2.5 ± 1.8 mV and 4.2 ± 2.8 mV, respectively (**Fig. 13C**). $V_{Osc, Mean}$ and $\Delta V_{Osc, Mean}$ were 1.0 ± 0.7 mV and 1.5 ± 1.1 mV, respectively (**Fig. 13C**). In a direct comparison of the magnitudes of slow and oscillatory components for each neuron-odor pair, ΔV_{Slow} exceeded $V_{Osc, Mean}$ and $\Delta V_{Osc, Mean}$ by a factor of 23.3 ± 20.6 and 15.7 ± 13.8, respectively. The 10 % largest fluctuations were exceeded by factors of 9.0 ± 5.7 ($V_{Osc, Max}$) and 5.2 ± 3.2 ($\Delta V_{Osc, Max}$). The average difference between the resting potential and the action potential threshold (ΔAP) was 29.0 ± 6.5 mV. Hence, using different means of quantification I found the amplitude of the oscillatory membrane potential fluctuations to be small compared to the slow component and compared to the depolarization required to reach spike threshold.

To further examine the mechanisms that drive Dp neurons towards action potential threshold, I examined subthreshold and suprathreshold odor responses of the same neuron in more detail. I compared ΔV_{Slow}, $V_{Osc, Mean}$ and $\Delta V_{Osc, Mean}$ for responses with no action potentials and with at least two action potentials. In suprathreshold responses (n = 12 recordings) ΔV_{Slow} was

significantly larger ($p < 0.0001$, Wilcoxon rank sum test) than in subthreshold responses (n = 20 recordings). ΔV_{Slow} amounted to 26.0 ± 5.6 mV and 17.5 ± 2.7 mV, respectively. $V_{Osc,\ Mean}$ and $\Delta V_{Osc,\ Mean}$ also increased but this difference was small (0.7 and 0.9 mV respectively) compared to the difference in ΔV_{Slow} (8.5 mV). Furthermore, the quantification of $V_{Osc,\ Mean}$ and $\Delta V_{Osc,\ Mean}$ may be slightly biased towards higher values in suprathreshold responses by residual contributions from action potentials after median filtering. I therefore conclude that temporal integration of synaptic inputs is required for action potential generation by Dp neurons and firing depends primarily on the amplitude of the slow component, while oscillatory components have only a minor influence.

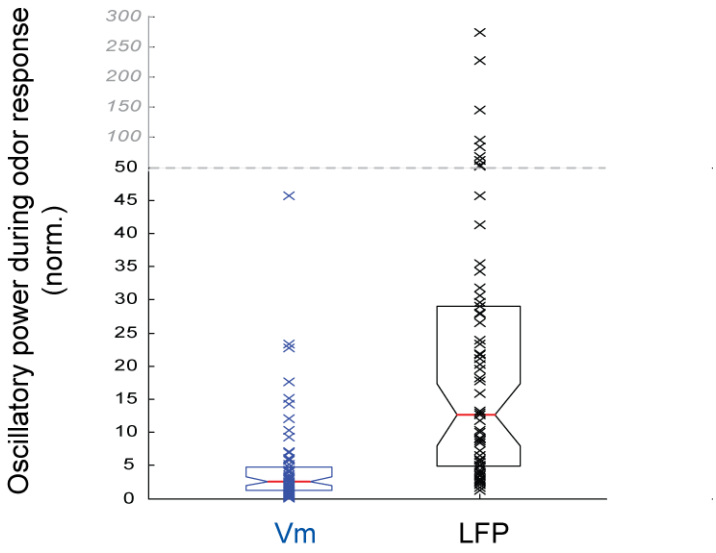

Figure 12: Oscillatory power of LFP and membrane potential during odor response.

Left: Odor-evoked change in power around the oscillation frequency in membrane voltage. Right: Odor-evoked change in power around the oscillation frequency in the LFP. Horizontal lines in the center of the boxes represent the median, the vertical extent of the boxes delineates the interquartile range. Notches show 95 % confidence intervals.

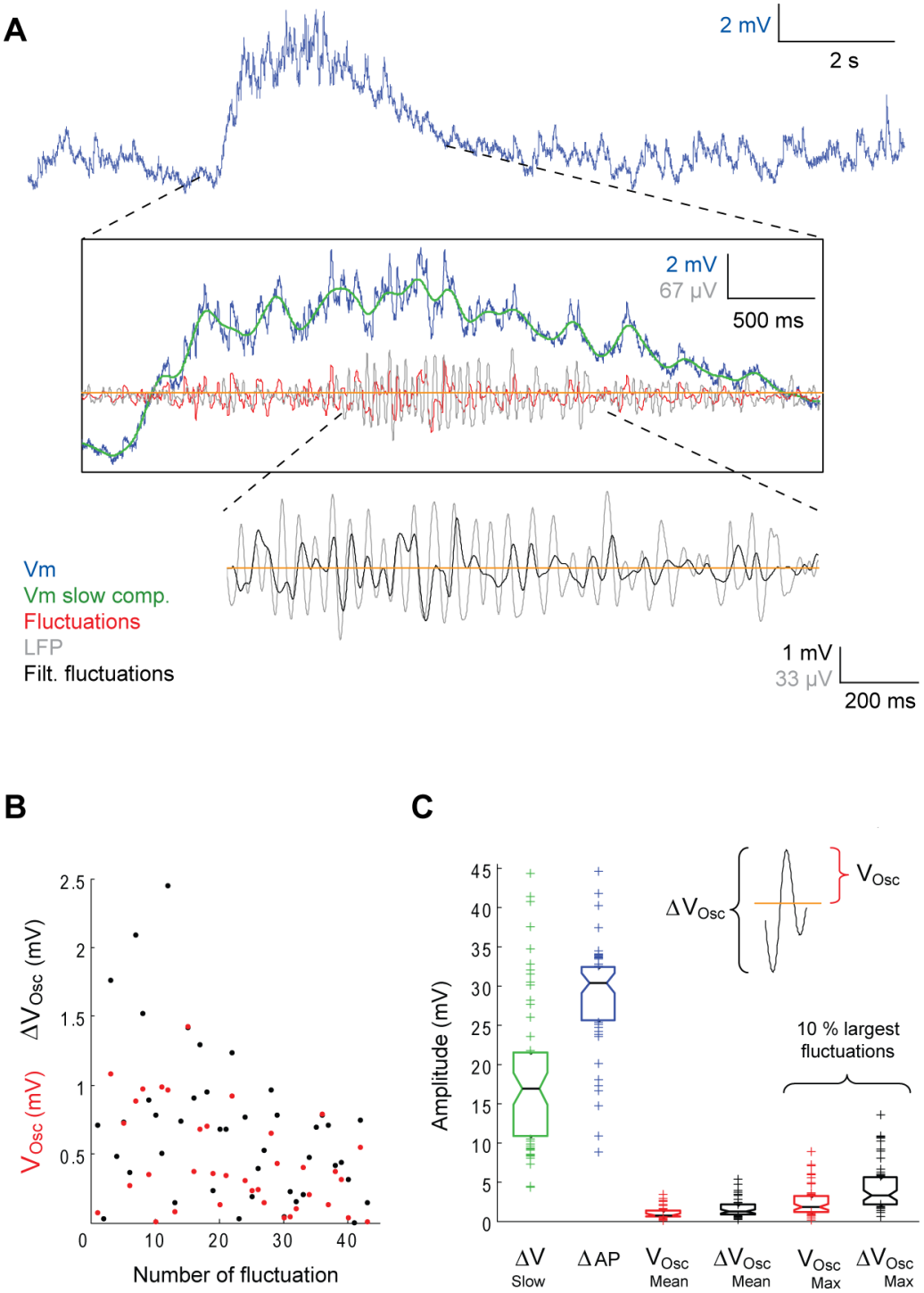

Figure 13: (Legend see next page)

Figure 13: Contribution of fast oscillatory fluctuations to the overall membrane depolarization.

(A) Top: Membrane potential response to stimulation with food extract. The magnitudes of the slow membrane depolarization and the fast oscillatory fluctuations were quantified individually after filtering of the original trace as illustrated at higher zoom in the inset. The green line shows the 5 Hz low-pass filtered trace used to estimate the slow depolarization. The red line is the difference between the original trace and the low-pass filtered trace. The band-pass filtered LFP is overlaid (gray). The zero-line is indicated in orange. The expanded inset shows an overlay of the LFP and the fast fluctuations after band-pass filtering at 5 – 40 Hz.

(B) Scatter plot of the amplitudes of individual fluctuations, maxima (V_{Osc}) and peak-to-peak amplitudes (ΔV_{Osc}), obtained from the recording in (A).

(C) Box plots summarizing the amplitudes of slow membrane depolarizations (ΔV_{Slow}), the relative membrane depolarization necessary to reach action potential threshold (ΔAP) and the amplitudes of fast fluctuations (V_{Osc}) for all 66 cell-odor pairs. Fast fluctuations were quantified by the mean maxima ($V_{Osc, Mean}$) and the mean peak-to-peak amplitudes ($\Delta V_{Osc, Mean}$) for each cell-odor pair. Average values for only the 10 % largest maxima ($V_{Osc, Max}$) and peak-to-peak amplitudes ($\Delta V_{Osc, Max}$) are shown in addition. Horizontal lines in the center of the boxes represent the median; the vertical extent of the boxes delineates the interquartile range. All data points outside the interquartile range are indicated. Notches indicate 95 % confidence intervals.

DISCUSSION

Sensory information detected at the periphery is transformed between successive processing stages to finally create a percept of the external environment. Here I explored the mechanisms that neuronal circuits in a higher olfactory brain area use to extract information from the output activity of the olfactory bulb.

Complex integration of olfactory inputs in Dp

I used 2-photon imaging of somatic Ca^{2+} signals to quantify mixture responses of individual Dp neurons. Ca^{2+} signals measured by this method are closely related to action potential firing in neurons of the adult zebrafish brain (Yaksi & Friedrich, 2006) and other brain areas (e.g. the mammalian neocortex, see Kerr et al, 2005). Thus, this technique provides a quantitative and reliable readout of neuronal activity.

Responses of Dp neurons to binary mixtures often resemble neither of the component responses. In the OB, in contrast, MC responses to binary mixtures are usually similar to one of the component responses. This "component dominance" for mixture representations in the OB has first been observed by electrophysiological recordings from mitral cells (Giraudet et al, 2002; Tabor et al, 2004) and has subsequently been confirmed by 2-photon Ca^{2+} - imaging using the same procedures as in this study (Yaksi et al, 2009). I therefore conclude that the mixture interactions observed in Dp cannot be explained by interactions at the level of the OB. While in the OB mixture responses are to a large extent determined by the component responses, mixture interactions in Dp indicate that odor responses in Dp neurons result from the integration of multiple sensory inputs and are shaped by the neuronal circuitry within Dp.

Convergence and synergism of diverse excitatory inputs

My data provides interesting and novel insights into the processing of sensory inputs by the neuronal circuitry in Dp.

1. Inputs from multiple MCs converge onto individual Dp neurons. The following evidence was found for this:

- Amino acids and bile acids, which activate distinct MC populations in the OB, frequently evoke subthreshold responses in the same Dp neuron.

- Mixture interactions observed for mixtures of one amino acid and one bile acid (**Fig. 4B**) are similar to those observed for mixtures of two amino acids (**Fig. 4A**).

- Intracellular recordings show a very broad subthreshold tuning (**Fig. 7**), implying that individual Dp neurons receive inputs from multiple MCs.

It remains to be explored whether this input convergence is direct or multisynaptic.

2. The topographic segregation of sensory inputs observed in the OB is not mapped onto the population of Dp neurons.

This is suggested by subthreshold responses to diverse molecular features often observed in the same Dp neuron and is a further conclusion from the findings that (i) responses to amino acids and bile acids, two stimulus classes that evoke non-overlapping responses in the OB, are often observed in the same Dp neuron and that (ii) mixture interactions occur for binary mixtures of one amino acid and one bile acid. Consistent with this conclusion, recent measurements of population activity patterns in Dp directly demonstrate that,

unlike in the OB, there is little or no topographic segregation of responses to different stimulus classes in Dp (Yaksi et al, 2009).

3. Afferent inputs may act synergistically to drive Dp neurons to spike threshold. This would explain part of the observed mixture interactions such as the observed strong mixture synergism and, particularly, the selective responses to binary mixtures but not their components.

Input convergence and synergistic activation of Dp neurons can, however, not explain all of my observations. In particular, additional mechanisms must be involved to achieve mixture suppression, and these might also account for the fact that mixture responses often fall in between the component responses.

Inhibitory control of odor responses

Component-selective responses and the frequently observed mixture suppression imply that odor responses in Dp are controlled by inhibition. The disinhibitory effect of Gabazine confirmed this conclusion and revealed that inhibition is mediated, at least partially, by GABAergic mechanisms involving $GABA_A$ receptors, consistent with observations in the piriform cortex of rodents (Franks & Isaacson, 2006; Luna & Schoppa, 2008).

In addition, I found that subthreshold depolarizing responses are reversed upon intracellular current injection, indicating that the membrane potential during the odor response is set primarily by the reversal potential of synaptically activated conductances. Since this reversal potential is near the threshold for action potential initiation, synaptic inputs most likely consist of a mixture of excitation and inhibition. Hence, odor responses of Dp neurons are not merely the result of a summation of excitatory inputs, but controlled by a balance of inhibitory and excitatory conductances. Moreover, the time courses of the odor responses in the absence and presence of current injection indicate that excitatory and inhibitory synaptic inputs follow different time courses.

In summary, response properties of Dp neurons are complex and seem to be shaped by convergent combinations of multiple excitatory and inhibitory synaptic inputs that cooperatively clamp the membrane potential to a defined, odor-dependent value close to spike threshold. The excitatory synaptic inputs may originate from mitral cells, intracortical connections, or combinations of both. In, contrast, inhibitory activity is most likely mediated exclusively by intracortical connections (Luna & Schoppa, 2008) (Y.-P. Zhang and R. W. Friedrich, unpublished observations). The neuronal circuitry in Dp therefore generates odor-specific patterns of excitation and inhibition from diverse afferent olfactory bulb input patterns. Thus, Dp may extract information about precise odorant features from MC activity patterns and mediate associations between segregated channels in the OB. This may allow Dp to transform the analytical representation of olfactory inputs in the OB into a synthetic olfactory image.

Mixture interactions in other brain areas

Recently, binary mixture responses were also examined by 2-photon Ca^{2+} -imaging in a subpallial target area of the OB, the ventral part of the ventral telencephalon (Vv) (Yaksi et al, 2009). Unlike neurons in the OB or Dp, neurons in Vv rarely showed mixture- or component- selective responses while mixture synergism was observed frequently. Moreover, Vv neurons were much more broadly tuned than neurons in the OB or in Dp. This demonstrates that different areas within the zebrafish telencephalon use distinct strategies to extract information from the OB output activity.

In insects, transformations of odor-encoding activity patterns between the antennal lobe and the mushroom body involve a combination of convergent excitatory input, multisynaptic inhibitory input and thresholding (Perez-Orive et al, 2002; Turner et al, 2008), suggesting that higher-order neuronal circuits in insects and vertebrates share basic features. Unlike in the

mushroom body, however, odor-evoked activity in Dp does not seem to be ultra-sparse. Thus, while the mushroom body and Dp may have common organizational principles at the level of afferent projections, the neuronal output appears to differ between the two brain areas. This suggests that distinct integration mechanisms may operate in higher brain centers of insects and vertebrates.

In the olfactory cortex of mammals, individual neurons integrate inputs originating from different mitral cells (Arenkiel et al, 2007; Franks & Isaacson, 2006; Wilson et al, 2006), receive excitatory and inhibitory inputs (Luna & Schoppa, 2008; Neville & Haberly, 2004) and show mixture suppression and synergism (Barnes et al, 2008; Yoshida & Mori, 2007; Zou & Buck, 2006), consistent with properties of Dp neurons. Major principles of sensory information processing in higher brain areas might thus be conserved across vertebrates but more detailed investigations are necessary to further address this issue.

Temporal properties of olfactory processing in Dp

To obtain further insights into the mechanisms that trigger stimulus-evoked action potentials in the olfactory circuitry in Dp, I investigated whether neurons in Dp may be explicitely sensitive to synchronized input from mitral cells in the OB. Information contained in the synchronization of action potentials may be read out by downstream neurons if these are endowed with mechanisms that selectively extract coincident synaptic inputs. I therefore examined whether Dp neurons differentiate between rhythmically synchronized and randomly timed inputs. In summary, I found no evidence for a selective filtering or amplification of rhythmically synchronized inputs by passive or active membrane properties. During odor stimulation, a signature of oscillatory MC activity may be preserved in the subthreshold membrane potential of Dp neurons, but action potential firing appears to depend primarily

on a slow depolarization that is independent of the fast oscillatory synchronization. These results indicate that Dp does not selectively extract information from the synchronization of MCs. Instead, Dp neurons integrate action potentials over tens of milliseconds or even longer time scales. An oscillatory temporal patterning in the inputs may, however, be partially preserved in action potential responses of Dp neurons.

Biophysical properties of Dp neurons favor temporal integration

Membrane time constants of Dp neurons are relatively long compared to the oscillation period (~50 ms) and to the precision of action potential synchronization of MCs (~5 ms) (Friedrich et al, 2004). In addition, impedance measurements revealed no selective amplification of frequencies around the oscillation frequency.

A potential limitation of the experimental approach is that whole-cell patch-clamp offers poor control over the voltage in distal parts of the dendritic tree. However, this is unlikely to mask coincidence detection mechanisms because the input resistance of the cells is relatively high, suggesting that cells are electrotonically compact. Furthermore, injection of sinusoidal currents did readily reveal frequency-specific amplification of input currents in other cell types (Haas & White, 2002; Hutcheon et al, 1996; Leung & Yu, 1998; Pike et al, 2000; Puil et al, 1986). My results therefore predict that responses of Dp neurons should not strongly depend on the synchronization of input currents on the millisecond time scale.

Consistent with this prediction, preliminary results indicate that the spike output produced by simulated trains of excitatory postsynaptic currents does not vary much with the synchronization of input currents. Individual Dp neurons are therefore unlikely to perform coincidence detection operations on a millisecond time scale. Rather, Dp neurons appear to act as a passive lowpass-filters with relatively long time constants. These results do not

exclude the possibility that a subpopulation of Dp neurons exhibits different active and passive membrane properties (Suzuki & Bekkers, 2006). However, if such neurons exist, they are likely to be the minority.

Dp neurons have a low spontaneous firing rate and high input resistances, similar to Kenyon cells in the insect mushroom body. Unlike Kenyon cells (Laurent & Naraghi, 1994), however, Dp neurons do not appear to amplify synchronous inputs. It will be interesting to compare the properties of Dp neurons to neurons in the mammalian olfactory cortex, in particular piriform cortex. To my knowledge, however, no published study has directly investigated active frequency-dependent membrane properties of neurons in the vertebrate olfactory cortex.

Odor responses are dominated by slow membrane depolarizations

Synchronized activity may also be detected by neuronal circuits, rather than by individual neurons. Studies in brain slices for example indicate that a sharply defined time window for the integration of excitatory inputs may be created by the time delay between monosynaptic excitatory input and polysynaptic feedforward inhibition. This has been demonstrated for pyramidal cells in the piriform cortex (Franks & Isaacson, 2006; Luna & Schoppa, 2008) and hippocampus (Pouille & Scanziani, 2001), and for Purkinje cells in the cerebellum (Mittmann et al, 2005). It remains, however, unclear whether this mechanism results in the selective detection of synchronized MC activity during an odor response in the intact brain. I therefore took advantage of the intact zebrafish olfactory system to investigate this question.

During an odor response, a subset of Dp neurons shows subthreshold oscillatory membrane potential activity that is phase-locked to the LFP oscillation in the OB. The amplitude of these membrane potential fluctuations is, however, small compared to a slow membrane depolarization. Moreover, the amplitude of the slow depolarization varies greatly between sub- and

suprathreshold responses, while the amplitude of the small fluctuations varies much less. I therefore conclude that the slow component of the response, which most likely reflects the gradual summation of synaptic inputs, is the most important determinant of action potential firing in Dp neurons. This slow summation is controlled by the balance of odor-evoked excitation and inhibition, as discussed above. Together, my results therefore indicate that the synchronization of inputs has little effect on the tuning of Dp neurons to odorants.

Although oscillations in the input appear to have little influence on the responsiveness of Dp neurons, it is nevertheless possible or even likely that the oscillatory temporal structure in the input influences the timing of action potentials by determining the exact time points when spike threshold is crossed. Some weak oscillatory spike timing may therefore be present in Dp. Investigating this would require further recordings of odor-evoked spikes and LFP oscillations, which is difficult because the spiking probability of Dp neurons is low.

Additional insights into the network mechanisms shaping odor responses in Dp may be obtained by investigating the relative timing of excitatory and inhibitory inputs. Electrophysiological recordings of odor-evoked voltage responses indicate that the time course of excitatory and inhibitory inputs is different but does not show prominent oscillatory rhythms (**Fig. 7A**). This is supported by the observation that recordings at different voltages after injection of a holding current are distinct and not mirror symmetric (**Fig. 7C**). It will thus be interesting to examine the relative timing of excitation and inhibition with more precision in voltage-clamp experiments.

Insect Kenyon cells detect coincident inputs not only by membrane intrinsic mechanisms, but also because feedforward-inhibition restrains the integration time window within each oscillation cycle. Consequently, membrane potential fluctuations and action potentials of Kenyon cells are

tightly phase-locked to the LFP oscillation. A feedforward inhibitory synaptic pathway is likely to exist also for the afferent input to Dp neurons (Y.-P. Zhang and R. W. Friedrich, unpublished observations). However, unlike in Kenyon cells, oscillatory membrane potential fluctuations are small and do not appear to contribute much to the overall spiking probability.

The piriform cortical circuitry also contains feed-forward inhibitory motifs that may narrow the integration time window(s) for excitatory inputs (Franks & Isaacson, 2006; Luna & Schoppa, 2008). These have been suggested to tune pyramidal cell responses to synchronous inputs from MCs. Nevertheless, the potential of this feedforward inhibition to shape oscillatory activity over several cycles remains to be addressed. Hence, further studies are required to examine whether the circuitry in the piriform cortex ensures a selective readout of synchronous MC spikes.

Readout of mitral cell activity patterns in Dp

My results indicate that responses of Dp neurons are not exquisitely sensitive to synchronized inputs but are primarily controlled by the balance between relatively slow excitatory and inhibitory inputs. In the temporal domain, Dp therefore appears to integrate afferent inputs over time. Since the majority of action potentials in the OB is not phase-locked to the LFP, at least for amino acid stimuli (Friedrich et al, 2004), Dp is likely to extract information contained in non-synchronized as well as synchronized MC activity patterns. These activity patterns contain information about the identity of odorants whereas an isolation of synchronized MC spikes would be informative about odor category (Friedrich et al, 2004).

Population response patterns of synchronized MC spikes tend to be highly correlated in response to odorants of the same category (Friedrich et al, 2004). Response patterns comprising the residual, non-synchronized spikes (Friedrich et al, 2004) or the entire ensemble of MC spikes (Friedrich &

Laurent, 2001; Friedrich & Laurent, 2004) in contrast, are initially correlated for similar odorants but then undergo a decorrelation, resulting in distinct activity patterns after a few hundred milliseconds. Because Dp neurons are not exquisitely sensitive to synchronized input, we predict that population activity patterns in Dp evoked by different stimuli should be distinct and convey information about the precise identity of an odor. Low correlations in odor-evoked population activity patterns in Dp have indeed been found (Yaksi et al, 2009 and unpublished results) and underscore the idea that Dp extracts complex information from synchronized and non-synchronized MC spikes and thus, has the potential to establish synthetic representations of odor objects.

Functional relevance of the temporal structure in the OB output

The slow temporal integration in Dp neurons raises the question about the relevance of the temporal structure in the OB output. As indicated by the analysis of mixture responses (Yaksi et al, 2009), different areas in the zebrafish telencephalon extract distinct information from MC spikes by distinct integration strategies. Thus, neurons in other brain areas may selectively read information from synchronized MC spikes and thereby extract information about odor category. Complementary information could then be synthesized at a later stage in olfactory processing. It will be interesting to study the temporal response properties of neurons in other brain regions such as Vv.

My data indicate that while the temporal structure in the MC output pattern does not appear to play a major role in tuning odor responses in Dp it is nevertheless maintained to some extent in the subthreshold membrane potential fluctuations. Information conveyed by the oscillatory temporal structure in the MC activity is thus not necessarily lost in Dp. Oscillatory synchrony may therefore be involved in yet unexplored processes such as sensory processing downstream of Dp or in mediating plastic changes required for learning and memory within Dp.

Consistent with earlier findings reporting that the onset of MC responses precedes LFP oscillations in the OB (Friedrich et al, 2004; Friedrich & Laurent, 2001) I observed that the odor-evoked depolarization of Dp neurons often reaches its peak before the LFP oscillation (not shown). Also in other vertebrates, particularly in the rabbit OB, it has been observed that spike discharges of mitral/tufted cells start before the LFP oscillation (Kashiwadani et al, 1999). This raises the possibility that OB output neurons activate higher order neurons, which then send feedback to the OB to generate the oscillations (Li & Hertz, 2000). However, even though centrifugal projections can modulate amplitude and frequency of OB oscillations (Gray & Skinner, 1988) it has been shown that they are not required for the oscillations to occur (Gray & Skinner, 1988).

To further explore a possible role of the odor-evoked rhythmical MC synchronization for the representation of odorants in Dp it would be interesting to compare odor responses in Dp neurons prior to and after selective elimination of oscillatory synchrony in the OB. LFP oscillations have been successfully disrupted by pharmacological interventions in the antennal lobes of locusts and honeybees. In locusts this disruption changed neither the response profiles nor the specificities of projection neurons (MacLeod & Laurent, 1996) while in behavioral experiments in honeybees it resulted in an impairment of fine sensory discrimination (Stopfer et al, 1997). In zebrafish, however, pharmacological disruption of the LFP causes epileptiform activity (Tabor et al, 2008) and is therefore not suitable for further investigations on the role of oscillatory synchronization.

From the data acquired during my PhD I conclude that individual neurons in Dp integrate information about diverse molecular features over time. Spikes are triggered by the temporal summation of activity from specific and distributed input channels while other input channels are silent. The neuronal circuitry in Dp is thus suitable to establish synthetic representations

of complex odor objects from highly analytical sensory inputs. The pronounced mixture interactions may provide a first mechanistic understanding for the fact that odorant mixtures are often perceived as distinct from the individual components (Jinks & Laing, 2001; Staubli et al, 1987).

Outlook

Genetic tools are emerging to dissect neuronal populations in the zebrafish telencephalon. This will allow to further address the functional role of excitatory and inhibitory circuits in shaping odor representations in higher olfactory brain areas. In addition it will give new insights into the role of neuromodulatory transmitter systems on the population dynamics in the intact brain. Advanced genetic tools, partially already available for mammalian model systems, will even offer control over specific subsets of neurons by targeted activation or inactivation.

Tracing studies of MC axons will be rewarding to quantify anatomical projections to individual higher order neurons and to explore the mapping of OB outputs onto the network in Dp. Such anatomical data is relevant to further advance a theoretical model of the olfactory system which may illuminate key principles governing information processing in neuronal networks.

Importantly, a further development of behavioral paradigms will be necessary to validate any systems level conclusions made in the ex-vivo preparation and to put the temporal structure of olfactory processing into the context of perception.

ABBREVIATIONS

Dp:	Posterior part of the dorsal telencephalon
LFP:	Local field potential
MC(s):	Mitral cell(s)
OB:	Olfactory bulb
PSD:	Power spectral density
SD:	Standard deviation
Vv:	Ventral part of the ventral telencephalon

REFERENCES

Ache BW, Young JM (2005) Olfaction: diverse species, conserved principles. *Neuron* **48:** 417-430

Adrian ED (1942) Olfactory reactions in the brain of the hedgehog. *J Physiol* **100:** 459-473

Alioto TS, Ngai J (2005) The odorant receptor repertoire of teleost fish. *BMC Genomics* **6**

Arenkiel BR, Peca J, Davison IG, Feliciano C, Deisseroth K, Augustine GJ, Ehlers MD, Feng G (2007) In vivo light-induced activation of neural circuitry in transgenic mice expressing channelrhodopsin-2. *Neuron* **54:** 205-218

Barnes DC, Hofacer RD, Zaman AR, Rennaker RL, Wilson DA (2008) Olfactory perceptual stability and discrimination. *Nat Neurosci* **11:** 1378-1380

Bernander Ö, Koch C, Usher M (1994) The effect of synchronized inputs at the single neuron level. *Neural Comput* **6:** 622-641

Borst A, Theunissen FE (1999) Information theory and neural coding. *Nat Neurosci* **2:** 947-957

Bressler SL (1987a) Relation of olfactory bulb and cortex. I. Spatial variation of bulbocortical interdependence. *Brain Res* **409:** 285-293.

Bressler SL (1987b) Relation of olfactory bulb and cortex. II. Model for driving of cortex by bulb. *Brain Res* **409:** 294-301.

Buonviso N, Revial MF, Jourdan F (1991) The Projections of Mitral Cells from Small Local Regions of the Olfactory Bulb: An Anterograde Tracing Study Using PHA-L (Phaseolus vulgaris Leucoagglutinin). *Eur J Neurosci* **3:** 493-500

Carr WES (1988) The molecular nature of chemical stimuli in the aquatic environment. In *Sensory biology of aquatic animals*, Atema J, Fay RR, Popper AN, Tavolga WN (eds), pp 3-27. New York: Springer

Denk W, Strickler JH, Webb WW (1990) Two-photon laser scanning fluorescence microscopy. *Science* **248:** 73-76

Desmaisons D, Vincent J-D, Lledo P-M (1999) Control of action potential timing by intrinsic subthreshold oscillations in olfactory bulb output neurons. *J Neurosci* **19:** 10727-10737

Eeckman FH, Freeman WJ (1990) Correlations between unit firing and EEG in the rat olfactory system. *Brain Res* **528:** 238-244

Finger TE (1975) The distribution of the olfactory tracts in the bullhead catfish, Ictalurus nebulosus. *J Comp Neurol* **161:** 125-141

Franks KM, Isaacson JS (2006) Strong single-fiber sensory inputs to olfactory cortex: implications for olfactory coding. *Neuron* **49:** 357-363

Friedrich RW, Habermann CJ, Laurent G (2004) Multiplexing using synchrony in the zebrafish olfactory bulb. *Nat Neurosci* **7:** 862-871

Friedrich RW, Korsching SI (1997) Combinatorial and chemotopic odorant coding in the zebrafish olfactory bulb visualized by optical imaging. *Neuron* **18:** 737-752

Friedrich RW, Korsching SI (1998) Chemotopic, combinatorial and noncombinatorial odorant representations in the olfactory bulb revealed using a voltage-sensitive axon tracer. *J Neurosci* **18:** 9977-9988

Friedrich RW, Laurent G (2001) Dynamic optimization of odor representations in the olfactory bulb by slow temporal patterning of mitral cell activity. *Science* **291:** 889-894

Friedrich RW, Laurent G (2004) Dynamics of olfactory bulb input and output activity during odor stimulation in zebrafish. *J Neurophysiol* **91:** 2658-2669

Friedrich RW, Yaksi E, Judkewitz B, Wiechert MT (2009) Processing of Odor Representations by Neuronal Circuits in the Olfactory Bulb. *Ann NY Acad Sci in press*

Frings S (2001) Chemoelectrical signal transduction in olfactory sensory neurons of air-breathing vertebrates. *Cell Mol Life Sci* **58:** 510-519

Giraudet P, Berthommier F, Chaput M (2002) Mitral cell temporal response patterns evoked by odor mixtures in the rat olfactory bulb. *J Neurophysiol* **88:** 829-838.

Gray CM, Skinner JE (1988) Centrifugal regulation of neuronal activity in the olfactory bulb of the waking rabbit as revealed by reversible cryogenic blockade. *Exp Brain Res* **69:** 378-386

Haas JS, White JA (2002) Frequency selectivity of layer II stellate cells in the medial entorhinal cortex. *J Neurophysiol* **88:** 2422-2429

Hara TJ (1994) The diversity of chemical stimulation in fish olfaction and gustation. *Rev Fish Biol Fish* **4:** 1-35

Hasselmo ME, Bower JM (1992) Cholinergic suppression specific to intrinsic not afferent fiber synapses in rat piriform (olfactory) cortex. *J Neurophysiol* **67:** 1222-1229

Hughes JR, Mazurowski JA (1962) Studies on the supracallosal mesial cortex of unanesthetized, conscious mammals. II. Monkey. B. Responses from the olfactory bulb. *Electroencephalogr Clin Neurophysiol* **14:** 635-645

Hutcheon B, Miura RM, Puil E (1996) Subthreshold membrane resonance in neocortical neurons. *J Neurophysiol* **76:** 683-697

Hutcheon B, Yarom Y (2000) Resonance, oscillation and the intrinsic frequency preferences of neurons. *Trends Neurosci* **23:** 216-222

Illig KR, Haberly LB (2003) Odor-evoked activity is spatially distributed in piriform cortex. *J Comp Neurol* **457:** 361-373.

Jinks A, Laing DG (2001) The analysis of odor mixtures by humans: evidence for a configurational process. *Physiol Behav* **72:** 51–63

Johnson DM, Illig KR, Behan M, Haberly LB (2000) New features of connectivity in piriform cortex visualized by intracellular injection of pyramidal cells suggest that "primary" olfactory cortex functions like "association" cortex in other sensory systems. *J Neurosci* **20:** 6974-6982

Joris P, Yin TC (2007) A matter of time: internal delays in binaural processing. *Trends in Neurosciences* **30:** 70-78

Kadohisa M, Wilson DA (2006) Separate encoding of identity and similarity of complex familiar odors in piriform cortex. *Proc Natl Acad Sci U S A* **103:** 15206-15211

Kashiwadani H, Sasaki YF, Uchida N, Mori K (1999) Synchronized oscillatory discharges of mitral/tufted cells with different molecular receptive ranges in the rabbit olfactory bulb. *J Neurophysiol* **82:** 1786-1792.

Kay LM, Stopfer M (2006) Information processing in the olfactory systems of insects and vertebrates. *Semin Cell Dev Biol* **17:** 433-442

Kerr JN, Greenberg D, Helmchen F (2005) Imaging input and output of neocortical networks in vivo. *Proc Natl Acad Sci U S A* **102:** 14063-14068

Ketchum KL, Haberly LB (1993) Synaptic events that generate fast oscillations in piriform cortex. *J Neurosci* **13:** 3980-3985.

Koch C, Rapp M, Segev I (1996) A brief history of time (constants). *Cereb Cortex* **6:** 93-101

Korsching S (2005) Selective imaging of the receptor neuron population in the olfactory bulb of zebrafish and mice. *Chem Senses* **30:** i101-102

Korsching SI (2001) Odor maps in the brain: spatial aspects of odor representation in the surface of the olfactory bulb. *Cell Mol Life Sci* **58:** 520-530

Laurent G (1996) Dynamical representation of odors by oscillating and evolving neural assemblies. *Trends Neurosci* **19:** 489-496

Laurent G (2002) Olfactory network dynamics and the coding of multidimensional signals. *Nat Rev Neurosci* **3:** 884-895

Laurent G, Naraghi M (1994) Odorant-induced oscillations in the mushroom bodies of the locust. *J Neurosci*

Leung LS, Yu HW (1998) Theta-frequency resonance in hippocampal CA1 neurons in vitro demonstrated by sinusoidal current injection. *J Neurophysiol* **79:** 1592-1596

Levine RL, Dethier S (1985) The connections between the olfactory bulb and the brain in the goldfish. *J Comp Neurol* **237:** 427-444

Li Z, Hertz J (2000) Odour recognition and segmentation by a model olfactory bulb and cortex. *Network* **11:** 83-102.

Lledo PM, Merkle FT, Alvarez-Buylla A (2008) Origin and function of olfactory bulb interneuron diversity. *Trends Neurosci* **31:** 392-400

Llinás RR (1988) The intrinsic electrophysiological properties of mammalian neurons: insights into central nervous system function. *Science* **242:** 1654-1664

Luna VM, Schoppa NE (2008) GABAergic Circuits Control Input-Spike Coupling in the Piriform Cortex. *J Neurosci* **28:** 8851-8859

MacLeod K, Laurent G (1996) Distinct mechanisms for synchronization and temporal patterning of odor-encoding neural assemblies. *Science* **274:** 976-979

Malnic B, Hirono J, Sato T, Buck LB (1999) Combinatorial receptor codes for odors. *Cell* **96:** 713-723

Mathieson WB, Maler L (1988) Morphological and electrophysiological properties of a novel in vitro preparation: the electrosenspry lateral line lobe brain slice. *J Comp Physiol A* **163:** 489-506

Mittmann W, Koch U, Häusser M (2005) Feed-forward inhibition shapes the spike output of cerebellar Purkinje cells. *J Physiol* **563:** 369-378

Mombaerts P, Wang F, Dulac C, Chao SK, Nemes A, Mendelsohn M, Edmondson J, Axel R (1996) Visualizing an olfactory sensory map. *Cell* **87:** 675-686

Mori K, Nagao H, Yoshihara Y (1999) The olfactory bulb: coding and processing of odor molecule information. *Science* **286:** 711-715

Mori K, Takahashi YK, Igarashi KM, Yamaguchi M (2006) Maps of odorant molecular features in the mammalian olfactory bulb. *Physiol Rev* **86:** 409-433

Nemenman I, Lewen GD, Bialek W, de Ruyter van Steveninck RR (2008) Neural coding of natural stimuli: information at sub-millisecond resolution. *PLoS Comput Biol* **4:** e1000025

Neville KR, Haberly LB (2004) Olfactory cortex. In *The synaptic organization of the brain*, Shepherd GM (ed), pp 415-454. Oxford: Oxford University Press

Ojima H, Mori K, Kishi K (1984) The trajectory of mitral cell axons in the rabbit olfactory cortex revealed by intracellular HRP injection. *J Comp Neurol* **230:** 77-87

Oram MW, Hatsopoulos NG, Richmond BJ, Donoghue JP (2001) Excess synchrony in motor cortical neurons provides redundant direction information with that from coarse temporal measures. *J Neurophysiol* **86:** 1700-1716

Perez-Orive J, Bazhenov M, Laurent G (2004) Intrinsic and circuit properties favor coincidence detection for decoding oscillatory input. *J Neurosci* **24:** 6037-6047

Perez-Orive J, Mazor O, Turner GC, Cassenaer S, Wilson RI, Laurent G (2002) Oscillations and sparsening of odor representations in the mushroom body. *Science* **297:** 359-365

Pike FG, Goddard RS, Suckling JM, Ganter P, Kasthuri N, Paulsen O (2000) Distinct frequency preferences of different types of rat hippocampal neurones in response to oscillatory input currents. *J Physiol* **529:** 205-213

Pologruto TA, Sabatini BL, Svoboda K (2003) ScanImage: flexible software for operating laser scanning microscopes. *Biomed Eng Online* **2:13**

Pouille F, Scanziani M (2001) Enforcement of temporal fidelity in pyramidal cells by somatic feed-forward inhibition. *Science* **293:** 1159-1163

Puil E, Gimbarzevsky B, Miura RM (1986) Quantification of membrane properties of trigeminal root ganglion neurons in guinea pigs. *J Neurophysiol* **55:** 995-1016

Rall W, Shepherd GM (1968) Theoretical reconstruction of field potentials and dendrodendritic synaptic interactions in olfactory bulb. *J Neurophysiol* **31:** 884-915.

Rennaker RL, Chen CF, Ruyle AM, Sloan AM, Wilson DA (2007) Spatial and temporal distribution of odorant-evoked activity in the piriform cortex. *J Neurosci* **27:** 1534-1542

Ressler KJ, Sullivan SL, Buck LB (1994) Information coding in the olfactory system: evidence for a stereotyped and highly organized epitope map in the olfactory bulb. *Cell* **79:** 1245-1255

Restrepo D, Teeter JH, Schild D (1996) Second messenger signaling in olfactory transduction. *J Neurobiol* **30:** 37-48

Rink E, Wullimann MF (2004) Connections of the ventral telencephalon (subpallium) in the zebrafish (Danio rerio). *Brain Res* **1011:** 206-220

Sato Y, Miyasaka N, Yoshihara Y (2007) Hierarchical regulation of odorant receptor gene choice and subsequent axonal projection of olfactory sensory neurons in zebrafish. *J Neurosci* **27:** 1606-1615

Satou M (1990) Synaptic organization, local neuronal circuitry, and functional segregation of the teleost olfactory bulb. *Prog Neurobiol* **34:** 115-142

Schild D, Restrepo D (1998) Transduction mechanisms in vertebrate olfactory receptor cells. *Physiol Rev* **78:** 429-466

Staubli U, Fraser D, Faraday R, Lynch G (1987) Olfaction and the "data" memory system in rats. *Behav Neurosci* **101:** 757-765

Stopfer M, Bhagavan S, Smith BH, Laurent G (1997) Impaired odour discrimination on desynchronization of odour-encoding neural assemblies. *Nature* **390:** 70-74

Stosiek C, Garaschuk O, Holthoff K, Konnerth A (2003) In vivo two-photon calcium imaging of neuronal networks. *Proc Natl Acad Sci U S A* **100:** 7319-7324

Suzuki N, Bekkers JM (2006) Neural coding by two classes of principal cells in the mouse piriform cortex. *J Neurosci* **26:** 11938-11947

Swadlow HA (2003) Fast-spike interneurons and feedforward inhibition in awake sensory neocortex. *Cereb Cortex* **13:** 25-32

Tabor R, Yaksi E, Friedrich RW (2008) Multiple functions of GABA(A) and GABA(B) receptors during pattern processing in the zebrafish olfactory bulb. *Eur J Neurosci* **28:** 117-127

Tabor R, Yaksi E, Weislogel JM, Friedrich RW (2004) Processing of odor mixtures in the zebrafish olfactory bulb. *J Neurosci* **24:** 6611-6620

Tang AC, Hasselmo ME (1994) Selective suppression of intrinsic but not afferent fiber synaptic transmission by baclofen in the piriform (olfactory) cortex. *Brain Res* **659:** 75-81

Turner GC, Bazhenov M, Laurent G (2008) Olfactory representations by Drosophila mushroom body neurons. *J Neurophysiol* **99:** 734-746

Uchida N, Takahashi YK, Tanifuji M, Mori K (2000) Odor maps in the mammalian olfactory bulb: domain organization and odorant structural features. *Nat Neurosci* **3:** 1035-1043

Ueno S, Bracamontes J, Zorumski C, Weiss DS, Steinbach JH (1997) Bicuculline and gabazine are allosteric inhibitors of channel opening of the GABAA receptor. *J Neurosci* **17:** 625-634

Vassar R, Chao SK, Sitcheran R, Nunez JM, Vosshall LB, Axel R (1994) Topographic organization of sensory projections to the olfactory bulb. *Cell* **79:** 981-991

von Bartheld CS, Meyer DL, Fiebig E, Ebbesson SO (1984) Central connections of the olfactory bulb in the goldfish, Carassius auratus. *Cell Tissue Res* **238:** 475-487

Wehr M, Laurent G (1996) Odor encoding by temporal sequences of firing in oscillating neural assemblies. *Nature* **384:** 162-166

Wilson DA (2003) Rapid, experience-induced enhancement in odorant discrimination by anterior piriform cortex neurons. *J Neurophysiol* **90:** 65-72

Wilson DA, Kadohisa M, Fletcher ML (2006) Cortical contributions to olfaction: plasticity and perception. *Semin Cell Dev Biol* **17:** 462-470

Wullimann MF, Mueller T (2004) Teleostean and mammalian forebrains contrasted: Evidence from genes to behavior. *J Comp Neurol* **475:** 143-162

Xu F, Greer CA, Shepherd GM (2000) Odor maps in the olfactory bulb. *J Comp Neurol* **422:** 489-495

Yaksi E, Friedrich RW (2006) Reconstruction of firing rate changes across neuronal populations by temporally deconvolved Ca^{2+} imaging. *Nat Methods* **3:** 377-383

Yaksi E, Judkewitz B, Friedrich RW (2007) Topological Reorganization of Odor Representations in the Olfactory Bulb. *PLoS Biol* **5:** e178

Yaksi E, von Saint Paul F, Niessing J, Bundschuh ST, Friedrich RW (2009) Transformation of odor representations in target areas of the olfactory bulb. *Nature Neurosci* **12:** 474-482

Yoshida I, Mori K (2007) Odorant category profile selectivity of olfactory cortex neurons. *J Neurosci* **27:** 9105-9114

Zhang X, Firestein S (2002) The olfactory receptor gene superfamily of the mouse. *Nat Neurosci* **5:** 124-133

Zou Z, Buck LB (2006) Combinatorial effects of odorant mixes in olfactory cortex. *Science* **311:** 1477-1481

Zou Z, Li F, Buck LB (2005) Odor maps in the olfactory cortex. *Proc Natl Acad Sci U S A* **102:** 7724-7729